# APPLICATION OF EQUILIBRIUM STATISTICAL MECHANICS TO ATMOSPHERES AND OCEANS

FREDDY BOUCHET

ANTOINE VENAILLE

*Ecole Normale Supérieure de Lyon et Université de Lyon 1, ENS-Lyon, Laboratoire de Physique, CNRS, 46 allée d'Italie, 69364 Lyon cedex 07, France.*
*Freddy.Bouchet@ens-lyon.fr*

We discuss statistical mechanics models of ocean and atmosphere flows. This theoretical approach explains the self-organization of turbulent flows described by the quasi-geostrophic equations, and predicts the output of their long time evolution. On these short lectures, emphasize has been placed on examples with available analytical treatment in order to favor better understanding of the physics and dynamics. We obtain quantitative models of the Great Red Spot and other Jovian vortices, ocean jets like the Gulf-Stream, ocean vortices, and we make quantitative predictions of vertical energy transfers in the ocean. A detailed comparison between these statistical equilibria and real flow observations or numerical simulations is provided.

## 1. Introduction

A striking and beautiful property of geophysical turbulent flows is their propensity to spontaneously self-organize into robust, large scale coherent structures. The most famous example is perhaps the Jovian Great Red Spot, an anticyclonic vortex observed many centuries ago. Similarly, the Earth's oceans are filled with long lived coherent structure: $300km$-diameter vortices with a ring shape are observed everywhere at the surface of the oceans. Mid-basin eastward jets, analogous to the Gulf-Stream or the Kuroshio exist in every oceanic basin, and strong bottom trapped recirculations such as the Zapiola anticyclone in the Argentine basin have been recently discovered. Understanding the physical mechanism underlying the formation and the persistence of these coherent structures in a turbulent flow remains a major theoretical challenge.

On the one hand, the problem of the self-organization of a turbulent flow involves a huge number of degrees of freedom coupled together via complex non-linear interactions. This situation makes any deterministic

approach illusory, if not impossible. On the other hand, there can be abrupt and drastic changes in the large scale flow structure when varying a single parameter such as the energy of the flow, or its circulation. It is then appealing to study this problem with a statistical mechanics approach, which reduces the problem of large-scale organization of the flow to the study of states depending on a few key parameters only. The first attempt to use equilibrium statistical mechanics ideas to explain the self-organization of 2D turbulence was performed by Onsager (1949) in the framework of the point vortex model. There exists now a theory, the Robert-Sommeria-Miller (RSM hereafter) equilibrium statistical mechanics, that explains the spontaneous organization of unforced and undissipated two-dimensional and geophysical flows (Robert, 1990; Miller, 1990; Robert, 1991; Robert and Sommeria, 1991). From the knowledge of the energy and the global distribution of potential vorticity levels provided by an initial condition, this theory predicts the large scale flow as the most probable outcome of turbulent mixing.

The aim of these lectures is to present applications of this equilibrium statistical mechanics theory specifically to the description of geophysical flows. There already exist several presentations of the equilibrium statistical mechanics of two-dimensional and geostrophic turbulent flows (Sommeria, 2001; Lim and Nebus, 2007; Majda and Wang, 2006), some emphasizing kinetic approaches of the point-vortex model (Chavanis, 2002), other focusing on the legacy of Onsager (Eyink and Sreenivasan, 2006). Interest of applications of statistical mechanics to climate problems is also discussed in a recent letter (Marston, 2011). A more detailed and precise explanation of the statistical mechanics basis of the RSM theory, actual computations of a large class of equilibrium states and further references can be found in a recent review (Bouchet and Venaille (2012)).

We present in the first section the quasi-geostrophic dynamics, a simple model for geophysical turbulent flows, and introduce the RSM statistical mechanics for this system. This theory is used to interpret the formation of Jovian vortices and oceanic rings in the second section, where a formal analogy between bubble formation and the self-organization phenomenon in geophysical flows is presented. The third section is devoted to the interpretation of eastward jets as marginal equilibrium states in oceanic basins. The last section deals with vertical energy transfers in geophysical flows, with application to the formation of bottom-trapped recirculations such as the Zapiola anticylone. The equilibrium statistical mechanics has a limited range of applicability since it neglects the effect of forcing and dissipation.

The validity of this hypothesis will be carefully addressed for each geophysical application in the related chapter, and will be discussed at a more general level in the conclusion.

## 2. Statistical mechanics of quasi-geostrophic flows

### 2.1. *The 1.5 layer quasi-geostrophic model*

We introduce here the simplest possible model for the dynamics of the Jovian atmosphere or the Earth's oceans: the quasi-geostrophic equations. There are several books discussing this model in more details, among which Gill (1982); Pedlosky (1982); Salmon (1998); Vallis (2006).

We assume that the dynamics takes place in an upper active layer, and there is a lower denser layer either at rest or characterized by a prescribed stationary current.

The flow is assumed to be strongly rotating with a Coriolis parameter $f = 2\Omega \sin\theta$, where $\theta$ is the latitude and $\Omega$ the rotation rate of the planet. Strongly rotating means that we consider the limit of small Rossby numbers $\epsilon = U/fL$, where $L$ is a typical length scale of the domain where the flow takes place, and $U$ is a typical velocity.

Another key quantity of this system is the Burger number $R/L$ where $R = \left(Hg\Delta\rho/\rho\right)^{1/2}/f$ is called the Rossby radius of deformation. It depends on the relative density difference $\Delta\rho/\rho$ between both layers, on the gravity $g$, on the Coriolis parameter $f$, and on the mean depth $H$ of the upper layer.

The fluids we consider are stably stratified, at hydrostatic balance on the vertical and at geostrophic balance on the horizontal. Geostrophic balance means that horizontal pressure gradients compensate the Coriolis force. These flows are called *quasi two-dimensional fluids* because one can show that the velocity field in the upper layer is horizontal and depth-independant (Taylor-Proudman theorem). In order to capture the dynamics, the quasi-geostrophic model is obtained through an asymptotic expansion of the Euler equations in the limit of small Rossby number $\epsilon$ (Pedlosky, 1982). The full dynamical system reads

$$\frac{\partial q}{\partial t} + \mathbf{v}\cdot\nabla q = 0, \quad \text{with } \mathbf{v} = \mathbf{e}_z \times \nabla\psi \ , \tag{1}$$

$$\text{and } q = \Delta\psi - \frac{\psi}{R^2} + \eta_d \ . \tag{2}$$

The complete derivation of the quasi-geostrophic equations shows that the streamfunction gradient $\nabla\psi$ is proportional to the pressure gradient along

the interface between the two layers. The dynamics (1) is a non-linear transport equation for a scalar quantity, the potential vorticity $q$ given by (2). The potential vorticity is a central quantity for geostrophic flows. The term $\Delta\psi = \omega$ is the relative vorticity[a].

The term $\psi/R^2$ is related to the interface pressure gradient and thus to the interface height variations through the hydrostatic balance. We see that $R$ appears as a characteristic length of the system. Although the rigorous derivation of quasi-geostrophic equations requires $R \sim L$, this model is commonly used in the regime $R \ll L$, either in numerical or theoretical works. This is usually a first step before considering the (more complex) shallow water equations which is the relevant model in this limit, see e.g. Pedlosky (1982).

The term $\eta_d = \beta y + \psi_d/R^2$ represents the combined effects of the planetary vorticity gradient $\beta y$ and of a given stationary flow $\psi_d$ in the deep layer. We assume that this deep flow is known and unaffected by the dynamics of the upper layer. The streamfunction $\psi_d$ induces a permanent deformation of the interface with respect to its horizontal position at rest[b]. This is why the deep flow acts as a topography on the active layer. The term $\beta y$ accounts at lowest order for the Earth's sphericity: the projection of the planet rotation vector on the local vertical axis is $f = 2\mathbf{\Omega} \cdot \mathbf{e}_z = f_0 + \beta y$, with $f_0 = 2\Omega \sin\theta_0$, where $\theta_0$ is the mean latitude where the flow takes place, and $\beta = 2\Omega \cos\theta_0/r_e$ with $r_e$ the planet's radius. This is called the beta-plane approximation because the term $\beta y$ appears as an effective topography in the quasi-geostrophic dynamics.

For the boundary conditions, two cases will be distinguished, depending on the domain geometry $\mathcal{D}$. In the case of a closed domain, there is an impermeability constraint (no flow across the boundary), which amounts to a constant streamfunction along the boundary. To simplify the presentation, the condition $\psi = 0$ at boundaries will be considered[c]. In the case of a

[a]The term "relative" refers to the vorticity $\omega$ in the rotating frame.

[b]A real topography $h(y)$ would correspond to $h = -f_0\eta_d/H$ where $f_0$ is the reference planetary vorticity at the latitude under consideration and $H$ is the mean upper layer thickness. Due to the sign of $f_0$, the signs of $h$ and $\eta_d$ would be the same in the south hemisphere and opposite in the north hemisphere. As we will discuss extensively the Jovian south hemisphere vortices, we have chosen this sign convention for $\eta_d$. We will consider the effect of a real topography when discussing vertical energy transfers, in the last section.

[c]The physically relevant boundary condition should be $\psi = \psi_{fr}$ where $\psi_{fr}$ is determined by using the mass conservation constraint $\int \mathrm{d}\mathbf{r}\ \psi = 0$ ($\psi$ is proportional to interface variations). Taking $\psi = 0$ does not change quantitatively the solutions in the domain

zonal channel, the streamfunction $\psi$ is periodic in the $x$ direction, and the impermeability constraint applies on northern and southern boundaries. In the remaining two sections, length scales are nondimensionalized such that the domain area $|\mathcal{D}|$ is equal to one.

Because we consider here a model with one active layer above another layer, it is called a 1.5 layer quasi-geostrophic model, which is also sometimes referred to as the "equivalent barotropic model".

### 2.2. *Dynamical invariants and their consequences*

According to Noether's Theorem, each symmetry of the system is associated with the existence of a dynamical invariant, see e.g. Salmon (1998). These invariants are crucial quantities, because they provide strong constraints for the flow evolution. Starting from (1), (2) and the aforementioned boundary conditions one can prove that quasi-geostrophic flows conserve the energy:

$$E = \frac{1}{2}\int_{\mathcal{D}} \mathrm{d}\mathbf{r}\, \left[(\nabla\psi)^2 + \frac{\psi^2}{R^2}\right] = -\frac{1}{2}\int_{\mathcal{D}} \mathrm{d}\mathbf{r}\, (q-\eta_d)\,\psi, \tag{3}$$

with $\mathbf{r} = (x, y)$. Additionally, the quasi-geostrophic dynamics (1) is a transport by an incompressible flow, so that the area $\gamma(\sigma)\, d\sigma$ occupied by a given vorticity level $\sigma$ is a dynamical invariant. The quantity $\gamma(\sigma)$ will be referred to as the global distribution of potential vorticity. The conservation of the distribution $\gamma(\sigma)$ is equivalent to the conservation of the Casimir's functionals $\int_{\mathcal{D}} \mathrm{d}\mathbf{r}\, f(q)$, where $f$ is any sufficiently smooth function.

Depending on the properties of the domain geometry where the flow takes place, the dynamics might be characterized by additional symmetries. Each of these symmetry would imply the existence of an additional invariant.

A striking consequence of the previous conservation laws is the fact that energy remains at large scale in freely evolving quasi-geostrophic dynamics. This property makes *a priori* possible the formation and the persistence of long lived coherent structures. This contrast with three dimensional turbulence, where the direct energy cascade (toward small scale) would rapidly dissipate such structures. These long lived coherent structures are by definition steady (or quasi-steady) states of the dynamics. The stationary points of the quasi-geostrophic equations (1), referred to as *dynamical equilibrium states*, satisfy $\mathbf{v}\cdot\nabla q = \nabla\psi\times\nabla q = 0$. It means that dynamical equilibria are flows for which streamlines are isolines of potential vorticity. Then,

bulk, but only the strength of boundary jets.

any state characterized by a $q-\psi$ functional relationship is a dynamical equilibrium. More details on the consequence of the conservation laws in two-dimensional and geophysical turbulent flows can be found in Bouchet and Venaille (2012).

At this point, we need a theory i) to support the idea that the freely evolving flow dynamics will effectively self-organize into a dynamical equilibrium state ii) to determine the $q-\psi$ relationship associated with this dynamical equilibrium iii) to select the dynamical equilibria that are likely to be observed. This is the goal and the achievement of equilibrium statistical mechanics theory, presented in the next subsection.

### 2.3. *The equilibrium statistical mechanics of Robert-Sommeria-Miller (RSM)*

The RSM statistical theory initialy developed by Robert (1990); Miller (1990); Robert (1991); Robert and Sommeria (1991) is introduced on a heuristic level in the following. There exist rigorous justifications of the theory see Bouchet and Venaille (2012) for detailed discussions and further references.

A microscopic state is defined by its potential vorticity field $q(\mathbf{r})$. If taken as an initial condition, such a fine grained field would evolve toward a state with filamentation at smaller and smaller scales, while keeping in general a well defined large scale organization. Then, among all the possible fine grained states, an overwhelming number are characterized by these complicated small scale filamentary structures. This phenomenology gives a strong incentive for a mean-field approach, in which the flow is described at a coarse-grained level. For that purpose, the probability $\rho(\sigma,\mathbf{r})\mathrm{d}\sigma$ is introduced to measure a potential vorticity level $\sigma$ at a point $\mathbf{r}=(x,y)$. The probability density field $\rho$ defines a macroscopic state of the system. The corresponding averaged potential vorticity field, also referred to as *coarse-grained*, or *mean-field*, is $\overline{q}\,(\mathbf{r})=\int_\Sigma \mathrm{d}\sigma\ \sigma\rho\,(\sigma,\mathbf{r})$, which is related to the streamfunction through $\overline{q}=\Delta\psi-\psi/R^2+\eta_d$, and where $\Sigma=]-\infty,\ +\infty[$.

Many microscopic states can be associated with a given macroscopic state. The cornerstone of the RSM statistical theory is the computation of the most probable state $\rho_{eq}$, that maximizes the Boltzmann-Gibbs (or mixing) entropy

$$\mathcal{S}\left[\rho\right]\equiv-\int_{\mathcal{D}}\mathrm{d}\mathbf{r}\int_\Sigma \mathrm{d}\sigma\,\rho\log\rho\ , \tag{4}$$

while satisfying the constraints associated with each dynamical invariant.

The mixing entropy (4) is a quantification of the number of microscopic states $q$ corresponding to a given macroscopic state $\rho$. The state $\rho_{eq}$ is not only the most probable one: an overwhelming number of microstates are effectively concentrated close to it (Michel and Robert, 1994). This gives the physical explanation and the prediction of the large scale organization of the flow.

To compute statistical equilibria, the constraints must be expressed in term of the macroscopic state $\rho$:

- The local normalization $N[\rho](\mathbf{r}) \equiv \int_\Sigma \mathrm{d}\sigma\ \rho(\sigma, \mathbf{r}) = 1$,
- The global potential vorticity distribution $D_\sigma[\rho] \equiv \int_\mathcal{D} d\mathbf{r}\, \rho(\sigma, \mathbf{r}) = \gamma(\sigma)$,
- The energy $\mathcal{E}[\rho] \equiv -\frac{1}{2}\int_\mathcal{D} \mathrm{d}\mathbf{r} \int_\Sigma \mathrm{d}\sigma\, \rho(\sigma - \eta_d)\,\psi = E$.

Because of the overwhelming number of states with only small scale fluctuations around the mean field potential vorticity, and because energy is a large scale quantity, contributions of these fluctuations to the total energy are negligible with respect to the mean-field energy.

The first step toward computations of RSM equilibria is to find critical points $\rho$ of the mixing entropy (4). In order to take into account the constraints, one needs to introduce the Lagrange multipliers $\zeta(\mathbf{r})$, $\alpha(\sigma)$, and $\lambda$ associated respectively with the local normalization, the conservation of the global vorticity distribution and of the energy. Critical points are solutions of:

$$\forall\ \delta\rho \quad \delta\mathcal{S} - \lambda\delta\mathcal{E} - \int_\Sigma \mathrm{d}\sigma\ \alpha\delta D_\sigma - \int_\mathcal{D} \mathrm{d}\mathbf{r}\ \zeta\delta N = 0\ , \tag{5}$$

where first variations are taken with respect to $\rho$. This leads to $\rho = N\exp(\lambda\sigma\psi(\mathbf{r}) - \alpha(\sigma))$ where N is determined by the normalization constraint $\left(\int \mathrm{d}\sigma\ \rho = 1\right)$. Statistical equilibria are dynamical equilibria characterized by a functional relation between potential vorticity and streamfunction:

$$\bar{q} = \frac{\int_\Sigma \mathrm{d}\sigma\ \sigma e^{\lambda\sigma\psi(\mathbf{r}) - \alpha(\sigma)}}{\int_\Sigma \mathrm{d}\sigma\, e^{\sigma\lambda\psi(\mathbf{r}) - \alpha(\sigma)}} = g(\psi) \tag{6}$$

It can be shown that $g$ is a monotonic and bounded function of $\psi$ for any global distribution $\gamma(\sigma)$ and energy $E$. These critical points can either be entropy minima, saddle or maxima. To find statistical equilibria, one needs then to select the entropy maxima.

At this point, two different approaches could be followed. The first one would be to consider a given small scale distribution $\gamma(\sigma)$ and energy

$E$, and then to compute the statistical equilibria corresponding to these parameters. In practice, especially in the geophysical context, one does not have empirically access to the microscopic vorticity distribution, but rather to the $q - \psi$ relation (6) of the large scale flow. The second approach, followed in the remaining of these lectures, is to study statistical equilibria corresponding to a given class of $q - \psi$ relations.

## 3. Statistical equilibria and jet solutions, application to ocean rings and to the Great Red Spot of Jupiter

Most analytical results on the equilibrium states are obtained in cases where the $q - \psi$ relation is close to be linear, or equivalently in the limit of a quadratic Energy-Casimir functional, see e.g. Bouchet and Venaille (2012) and references therein. More general solutions are very difficult to find analytically, and may require numerical computations, for instance using continuation algorithms.

There are however other limits where an analytical description becomes possible. This is for instance the case in the limit of large energies (Turkington, 1983). The second interesting limit is the limit of Rossby deformation radius $R$ much smaller than the size of the domain ($R \ll L$), where the nonlinearity of the vorticity-stream function relation becomes essential. This limit case and its applications to the description of coherent structures in geostrophic turbulence is the subject of this section.

In the limit $R \ll L$, the variational problems of the statistical theory are analogous to the Van-Der-Waals Cahn Hilliard model that describes phase separation and phase coexistence in usual thermodynamics. The Van-Der-Waals Cahn Hilliard model describes for instance the equilibrium of a bubble of a gas phase in a liquid phase, or the equilibria of soap films in air. For these classical problems, the essential concepts are the free energy per unit area, the related spherical shape of the bubbles, the Laplace equation relating the radius of curvature of the bubble with the difference in pressure inside and outside the bubble (see section 3.1), or properties of minimal surfaces (the Plateau problem). We will present an analogy between those concepts and the structures of quasi-geostrophic statistical equilibrium flows.

For these flows, the limit $R \ll L$ leads to interfaces separating phases of different free energies. In our case, each phase is characterized by a different value of average potential vorticity, and corresponds to sub-domains in which the potential vorticity is homogenized. The interfaces correspond

to strong localized jets of typical width $R$. This limit is relevant for applications showing such strong jet structures.

From a geophysical point of view, this limit $R \ll L$ is relevant for describing some of Jupiter's features, like for instance the Great Red Spot of Jupiter (a giant anticyclone) (here $R \simeq 500 - 2000\,km$ and the length of the spot is $L \simeq 20,000\,km$) (see section 3.3).

This limit is also relevant to ocean applications, where $R$ is the internal Rossby deformation radius ($R \simeq 50\,km$ at mid-latitude). We will apply the results of statistical mechanics to the description of robust (over months or years) vortices such as ocean rings, which are observed around mid-latitude jets such as the Kuroshio or the Gulf Stream, and more generally in any eddying regions (mostly localized near western boundary currents) as the Aghulas current, the confluence region in the Argentinian basin or the Antarctic Circumpolar circulation (see section 3.4). The length $L$ can be considered as the diameters of those rings ($L \simeq 200\,km$).

We will also apply statistical mechanics ideas in the limit $R \ll L$ to the description of the large scale organization of oceanic currents (in inertial region, dominated by turbulence), such as the eastward jets like the Gulf Stream or the Kuroshio extension (the analogue of the Gulf Stream in the Pacific ocean). In that case the length $L$ could be thought as the ocean basin scale $L \simeq 5,000\,km$ (see section 4).

### 3.1. *The Van der Waals–Cahn Hilliard model of first order phase transitions*

We first describe the Van der Waals–Cahn Hilliard model. We give in the following subsections a heuristic description based on physical arguments. Some comments and references on the mathematics of the problem are provided in section 3.1.4.

This classical model of thermodynamics and statistical physics describes the coexistence of phase in usual thermodynamics. It involves the minimization of a free energy with a linear constraint:

$$\left\{ \begin{array}{c} F = \min \left\{ \mathcal{F}\left[\phi\right] \;\middle|\; \mathcal{A}\left[\phi\right] = -B \right\} \\ \text{with} \;\; \mathcal{F} = \int_{\mathcal{D}} \mathrm{d}\mathbf{r} \, \left[ \frac{R^2 (\nabla \phi)^2}{2} + f(\phi) \right] \;\; \text{and} \;\; \mathcal{A}\left[\phi\right] = \int_{\mathcal{D}} \mathrm{d}\mathbf{r} \, \phi \end{array} \right. \tag{7}$$

where $\phi$ is the non-dimensional order parameter (for instance the non-dimensionality local density), and $f\left(\phi\right)$ is the non-dimensional free energy per unit volume. We consider the limit $R \ll L$ where $L$ is a typical size of the domain. We assume that the specific free energy $f$ has a double well

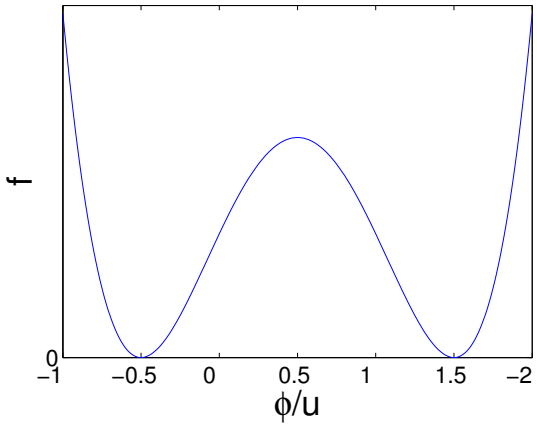


Figure 1. The double well shape of the specific free energy $f(\phi)$ (see equation (7)). The function $f(\phi)$ is even and possesses two minima at $\phi = \pm u$. At equilibrium, at zeroth order in $R$, the physical system will be described by two phases corresponding to each of these minima.

shape (see figure 1), characteristic of a phase coexistence related to a first order phase transition. For a simpler discussion, we also assume $f$ to be even; this does not affect the properties of the solutions discussed bellow.

### 3.1.1. *First order phase transition and phase separation*

At equilibrium, in the limit of small $R$, the function $f(\phi)$ plays the dominant role. In order to minimize the free energy, the system will tend to reach one of its two minima (see figure 1). These two minima correspond to the value of the order parameters for the two coexisting phases, the two phases have thus the same free energy.

The constraint $\mathcal{A}$ (see equation. 7) is related to the total mass (due to the translation on $\phi$ to make $f$ even, it can take both positive and negative values). Without the constraint $\mathcal{A}$, the two uniform solutions $\phi = u$ or $\phi = -u$ would clearly minimize $\mathcal{F}$: the system would have only one phase. Because of the constraint $\mathcal{A}$, the system has to split into sub-domains: part of it with phase $\phi = u$ and part of it with phase $\phi = -u$. In a two dimensional space, the area occupied by each of the phases are denoted $A_+$ and $A_-$ respectively. They are fixed by the constraint $\mathcal{A}$ by the relations $uA_+ - uA_- = -B$ and by $A_+ + A_- = 1$ (where 1 is the total area). A sketch of a situation with two sub-domains each occupied by one of the two

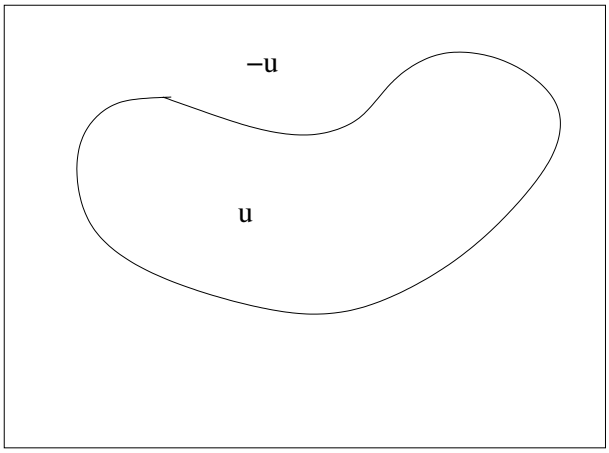


Figure 2. At zeroth order, $\phi$ takes the two values $\pm u$ on two sub-domains $A_{\pm}$. These sub-domains are separated by strong jets. The actual shape of the structure, or equivalently the position of the jets, is given by the first order analysis.

phases is provided in figure 2.

Up to now, we have neglected the term $R^2 (\nabla\phi)^2$ in the functional (7). In classical thermodynamics, this term is related to non-local contributions to the free energy (proportional to the gradient rather than to only pointwise contributions). Moreover the microscopic interactions fix a length scale $R$ above which such non-local interactions become negligible. Usually for a macroscopic system such non-local interactions become negligible in the thermodynamic limit. Indeed as will soon become clear, this term gives finite volume or interface effects.

We know from observations of the associated physical phenomena (coarsening, phase separations, and so on) that the system has a tendency to form larger and larger sub-domains. We thus assume that such sub-domains are delimited by interfaces, with typical radius of curvature $r$ much larger than $R$[d]. Actually the term $R^2 (\nabla\phi)^2$ is negligible except on an interface of width $R$ separating the sub-domains. The scale separation $r \gg R$ allows to consider independently what happens in the transverse direction to the interface on the one hand and in the along interface direction on the other hand. As described in next sections, this explains the interface structure and interface shape respectively.

[d]This can indeed be proved mathematically, see section 3.1.4

3.1.2. *The interface structure*

At the interface, the value of $\phi$ changes rapidly, on a scale of order $R$, with $R \ll r$. What happens in the direction along the interface can thus be neglected at leading order. To minimize the free energy (7), the interface structure $\phi(\zeta)$ needs thus to minimize a one dimensional variational problem along the normal to the interface coordinate $\zeta$

$$F_{int} = \min \left\{ \int \mathrm{d}\zeta \left[ \frac{R^2}{2} \left( \frac{d\phi}{d\zeta} \right)^2 + f(\phi) \right] \right\}. \tag{8}$$

Dimensionally, $F_{int}$ is a free energy $F$ divided by a length. It is the free energy per unit length of the interface.

We see that the two terms in (8) are of the same order only if the interface has a typical width of order $R$. We rescale the length by $R$: $\zeta = R\tau$. The Euler-Lagrange equation of (8) gives

$$\frac{d^2\phi}{d\tau^2} = \frac{df}{d\phi}. \tag{9}$$

This equation is a very classical one. For instance making an analogy with mechanics, if $\phi$ would be a particle position, $\tau$ would be the time, equation (9) would describe the conservative motion of the particle in a potential $V = -f$. From the shape of $f$ (see figure 1) we see that the potential has two bumps (two unstable fixed points) and decays to $-\infty$ for large distances. In order to connect the two different phases in the bulk, on each side of the interface, we are looking for solutions with boundary conditions $\phi \to \pm u$ for $\tau \to \pm\infty$. It exists a unique trajectory with such limit conditions: in the particle analogy, it is the trajectory connecting the two unstable fixed points (homoclinic orbit).

This analysis shows that the interface width scales like $R$. Moreover, after rescaling the length, one clearly sees that the free energy per length unit (8) is proportional to $R$: $F_{int} = eR$, where $e > 0$ could be computed as a function of $f$ (Bouchet and Sommeria, 2002; Venaille and Bouchet, 2011a).

3.1.3. *The interface shape: an isoperimetrical problem*

In order to determine the interface shape, we come back to the free energy variational problem (7). In the previous section, we have determined the transverse structure of the interface, by maximizing the one dimensional variational problem (8). We have discussed the quantity $F_{int} = Re$, a free

energy per unit length, which is the unit length contribution of the interface to the free energy. The total free energy is thus

$$\mathcal{F} = eRL, \tag{10}$$

where we have implicitly neglected contributions of relative order $R/r$, where $r$ is the curvature radius of the interface.

In order to minimize the free energy (10), we thus have to minimize the length $L$. We must also take into account that the areas occupied by the two phases, $A_+$ and $A_-$ are fixed, as discussed in section 3.1.1. We thus look for the curve with the minimal length, that bounds a surface with area $A_+$

$$\min \{eRL \,|\text{Area} = A_+ \}\,. \tag{11}$$

This type of problem is called an isoperimetrical problem. In three dimensions, the minimization of the area for a fixed volume leads to spherical bubbles or plane surface if the boundaries does not come into play. When boundaries are involved, the interface shape is more complex (it is a minimal surface -or Plateau- problem). This can be illustrated by nice soap films experiments, as may be seen in very simple experiments or in many science museums. Here, for our two dimensional problem, it leads to circle or straight lines, as we now prove.

It is a classical exercise of variational calculus to prove that the first variations of the length of a curve is proportional to the inverse of its curvature radius $r$. The solution of the problem (11) then leads to

$$\frac{eR}{r} = \alpha, \tag{12}$$

where $\alpha$ is a Lagrange parameter associated with the conservation of the area. This proves that $r$ is constant along the interface: solutions are either circles or straight lines. The law (12) is the equivalent of the Laplace law in classical thermodynamics, relating the radius of curvature of the interface to the difference of pressure inside and outside of the bubble[e].

We have thus shown that the minimization of the Van-Der-Waals Cahn Hilliard functional, aimed at describing statistical equilibria for first order phase transitions, predicts phase separation (formation of sub-domains with

[e]Indeed, at next order, the Lagrange parameter $\alpha$ leads to a slight imbalance between the two phase free energy, which is related to a pressure difference for the two phases. This thus gives the relation between pressure imbalance, radius of curvature and free energy per unit length (or unit surface in the 3D case).


Figure 3. Illustration of the Plateau problem (or minimal area problem) with soap films: the spherical bubble minimizes its area for a given volume (Jean Simeon Chardin, *Les bulles de savon*, 1734)

each of the two phases corresponding to the two minima of the free energy). It predicts the interface structure and that its shape is described by an isoperimetrical problem: the minimization of the length for a fixed enclosed area. Thus equilibrium structures are either bubbles (circles) or straight lines. In the following sections, we see how this applies to the description of statistical equilibria for quasi-geostrophic flows, describing vortices and jets.

### 3.1.4. *The mathematics of the Van-Der-Waals Cahn Hilliard problem*

The study of the Van-Der-Waals Cahn Hilliard functional (7) was a mathematical challenge during the 1980s. It's solution has followed from the analysis in the framework of spaces of functions with bounded variations, and on results from semi-local analysis. One of the main contributions to this problem was achieved by Modica (1987). This functional analysis study proves the assumptions of the heuristic presentation given in the pre-

vious subsections: $\phi$ takes the two values $\pm u$ in sub-domains separated by transition area of width scaling with $R$.

As a complement to these mathematical works, a more precise asymptotic expansion based on the heuristic description above, generalizable at all order in $R$, with mathematical justification of the existence of the solutions for the interface equation at all order in $R$, is provided in Bouchet (2001). Higher order effects are also discussed in this work.

### 3.2. *Quasi-geostrophic statistical equilibria and first order phase transitions*

The first discussion of the analogy between statistical equilibria in the limit $R \ll L$ and phase coexistence in usual thermodynamics, in relation with the Van-Der-Waals Cahn Hilliard model is given in Bouchet (2001); Bouchet and Sommeria (2002). This analogy has been recently put on a more precise mathematical ground, by proving that the variational problems of the RSM statistical mechanics and the Van-Der-Waals Cahn Hilliard variational problem are indeed related (Bouchet, 2008). More precisely, any solution to the variational problem:

$$\left\{ \begin{array}{c} F = \min \left\{ \mathcal{F}\left[\phi\right] \ | \ \mathcal{A}\left[\phi\right] = -B \right\} \\ \text{with} \ \ \mathcal{F} = \int_{\mathcal{D}} \mathrm{d}\mathbf{r} \left[ \frac{R^2 (\nabla \phi)^2}{2} + f\left(\phi\right) - R\phi h \right] \ \ \text{and} \ \ \mathcal{A}\left[\phi\right] = \int_{\mathcal{D}} \mathrm{d}\mathbf{r}\, \phi \end{array} \right. \tag{13}$$

where $\psi = R^2 \phi$ is a RSM equilibria of the quasi-geostrophic equations (1).

Considering the problem (13), using a part integration and the relation $q = R^2 \Delta \phi - \phi + Rh$ yields

$$\delta \mathcal{F} = \int \mathrm{d}\mathbf{r} \ \left( f'(\phi) - \phi - q \right) \delta \phi \quad \text{and} \quad \delta \mathcal{A} = \int \mathrm{d}\mathbf{r} \ \delta \phi. \tag{14}$$

Critical points of (13) are therefore solutions of $\delta \mathcal{F} - \alpha \delta \mathcal{A} = 0$, for all $\delta \phi$, where $\alpha$ is the Lagrange multiplier associated with the constraint $\mathcal{A}$. These critical points satisfy

$$q = f'\left( \frac{\psi}{R^2} \right) - \frac{\psi}{R^2} - \alpha.$$

We conclude that this equation is the same as (6), provided that $f'\left(\frac{\psi}{R^2}\right) = g(\beta\psi) + \frac{\psi}{R^2} - \alpha$.

In the case of an initial distribution $\gamma$ with only two values of the potential vorticity: $\gamma(\sigma) = |\mathcal{D}| \left( a\delta(\sigma_1) + (1-a)\delta(\sigma_2) \right)$, only two Lagrange multipliers $\alpha_1$ and $\alpha_2$ are needed, associated with $\sigma_1$ and $\sigma_2$ respectively,

in order to compute $g$, equation (6). In that case, the function $g$ is exactly tanh function. There exists in practice a much larger class of initial conditions for which the function $g$ would be an increasing function with a single inflexion point, similar to a tanh function, especially when one considers the limit of small Rossby radius of deformation. Bouchet and Sommeria (2002); Venaille and Bouchet (2011a) give physical arguments to explain why it is the case for Jupiter's troposphere or oceanic rings and jets.

When $g$ is a tanh-like function, the specific free energy $f$ has a double well shape, provided that the inverse temperature $\beta$ is negative, with sufficiently large values.

#### 3.2.1. *Topography and anisotropy*

The topography term $\eta_d = Rh\,(y)$ in (13) is the main difference between the Van-Der-Waals Cahn Hilliard functional (7) and the quasi-geostrophic variational problem (13). We recall that this term is due to the beta plane approximation and a prescribed motion in a lower layer of fluid (see section 2.1). This topographic term provides an anisotropy in the free energy. Its effect will be the subject of most of the theoretical discussion in the following sections.

Since we suppose that this term scales with $R$, the topography term will not change the overall structure at leading order: there will still be phase separations in sub-domains, separated by an interface of typical width $R$, as discussed in section 3.1. We now discuss the dynamical meaning of this overall structure for the quasi-geostrophic model.

#### 3.2.2. *Potential vorticity mixing and phase separation*

In the case of the quasi-geostrophic equations, the order parameter $\phi$ is proportional to the stream function $\psi$: $\psi = R^2\phi$. At equilibrium, there is a functional relation between the stream function $\psi$ and the macroscopic potential vorticity $q$, given by Eq. (6). Then the sub-domains of constant $\phi$ are domains where the (macroscopic) potential vorticity $q$ is also constant. It means that the level of mixing of the different microscopic potential vorticity levels are constant in those sub-domains. We thus conclude that the macroscopic potential vorticity is homogenized in sub-domains that corresponds to different phases (with different values of potential vorticity), the equilibrium being controlled by an equality for the associated mixing free energy.

3.2.3. *Strong jets and interfaces*

In section 3.1.3, we have described the interface structure. The order parameter $\phi$ varies on a scale of order $R$ mostly in the normal to the interface direction, reaching constant values far from the interface. Recalling that $\phi$ is proportional to $\psi$, and that $\mathbf{v} = \mathbf{e}_z \wedge \nabla\psi$, we conclude that:

(1) The velocity field is nearly zero far from the interface (at distances much larger than the Rossby deformation radius $R$). Non zero velocities are limited to the interface areas.
(2) The velocity is mainly directed along the interface.

These two properties characterize strong jets. In the limit $R \ll L$, the velocity field is thus mainly composed of strong jets of width $R$, whose path is determined from an isoperimetrical variational problem.

## 3.3. *Application to Jupiter's Great Red Spot and other Jovian features*

Most of Jupiter's volume is gas. The visible features on this atmosphere, cyclones, anticyclones and jets, are concentrated on a thin outer shell, the troposphere, where the dynamics is described by similar equations to the ones describing the Earth's atmosphere (Dowling, 1995; Ingersoll and Vasavada, 1998). The inner part of the atmosphere is a conducting fluid, and the dynamics is described by Magneto-hydrodynamics (MHD) equations.

The most simple model describing the troposphere is the 1-1/2 quasi-geostrophic model, described in section 2.1. This simple model is a good one for localized mid latitude dynamics. Many classical work have used it to model Jupiter's features, taking into account the effect of a prescribed steady flow in a deep layer acting like an equivalent topography $h\,(y)$. We emphasize that there is no real bottom topography on Jupiter.

Some works based on soliton theory aimed at explaining the structure and stability of the Great Red Spot. However, none of these obtained a velocity field qualitatively similar to the observed one, which is actually a strongly non-linear structure. Structures similar to the Great Red Spot have been observed in a number of numerical simulations, but without reproducing in a convincing way both the characteristic annular jet structure of the velocity field and the shape of the spot. Detailed observations and fluid mechanics analysis described convincingly the potential vorticity structure and the dynamical aspects of the Great Red Spot (see Dowling (1995); Ingersoll and Vasavada (1998); Marcus (1993) and references

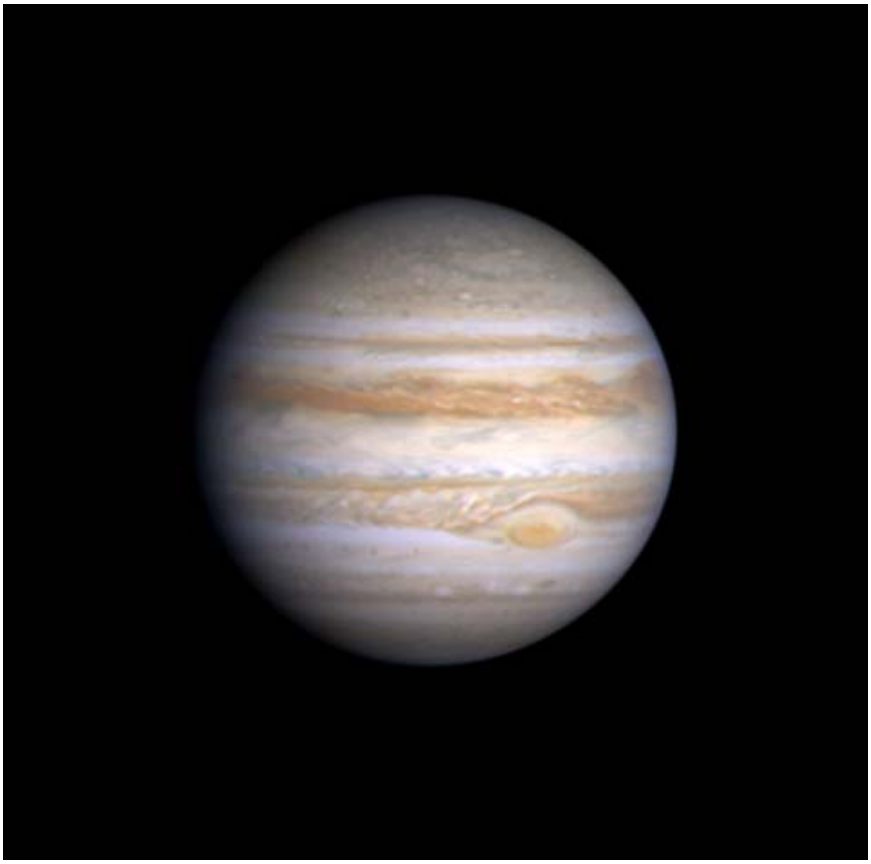

Figure 4. Observation of the Jovian atmosphere from Cassini (Courtesy of NASA/JPL-Caltech). One of the most striking feature of the Jovian atmosphere is the self organization of the flow into alternating eastward and westward jets, producing the visible banded structure and the existence of a huge anticyclonic vortex $\sim 20,000\ km$ wide, located around 20 South: the Great Red Spot (GRS). The GRS has a ring structure: it is a hollow vortex surrounded by a jet of typical velocity $\sim 100\ m.s^{\{-1\}}$ and width $\sim 1,000\, km$. Remarkably, the GRS has been observed to be stable and quasi-steady for many centuries despite the surrounding turbulent dynamics. The explanation of the detailed structure of the GRS velocity field and of its stability is one of the main achievement of the equilibrium statistical mechanics of two dimensional and geophysical flows (see figure 3.3 and section 3).

therein). The potential vorticity structure is a constant vorticity inside the spot surrounded by a gentle shear outside, which gives a good fluid mechanics theory (Marcus, 1993). In this section we explain this potential

vorticity structure thanks to statistical mechanics. Statistical mechanics provides also more detailed, and analytical theory of the shape of Jupiter vortices.

The explanation of the stability of the Great Red Spot of Jupiter using the statistical mechanics of the quasi-geostrophic model is cited by nearly all the papers from the beginning of the Robert-Sommeria-Miller theory. Some equilibria having qualitative similarities with the observed velocity field have been computed in Sommeria *et al.* (1991). The theoretical study in the limit of small Rossby deformation radius, especially the analogy with first order phase transitions (Bouchet and Sommeria, 2002; Bouchet and Dumont, 2003) gave the theory presented below: an explanation of the detailed shape and structure and a quantitative model. These results have been extended to the shallow-water model (Bouchet *et al.*, 2012). Turkington *et al.* (2001) argued on the explanation of the position of the Great Red Spot based on statistical mechanics equilibria.

We describe in the following the prediction of equilibrium statistical mechanics for the quasi-geostrophic model with topography. We start from the Van-Der-Waals Cahn Hilliard variational problem in presence of small topography (13), recalling that its minima are statistical equilibria of the quasi-geostrophic model (see section 3.2).

The Rossby deformation radius at the Great Red Spot latitude is evaluated to be of order of $500 - 2000$ km, which has to be compared with the size of the spot: $10,000\, X\, 20,000$ km. This is thus consistent with the limit $R \ll L$ considered in the description of phase coexistence within the Van-Der-Waals Cahn Hilliard model (section 3.1), even if the criteria $r \ll R$ is only marginally verified where the curvature radius $r$ of the jet is the larger.

In the limit of small Rossby deformation radius, the entropy maxima for a given potential vorticity distribution and energy, are formed by strong jets, bounding areas where the velocity is much smaller. Figure 3.3 shows the observation of the Great Red Spot velocity field, analyzed from cloud tracking on spacecraft pictures. The strong jet structure (the interface) and phase separation (much smaller velocity inside and outside the interface) is readily visible. The main difference with the structure described in the previous section is the shape of the vortex: it is not circular as was predicted in the case without topography or with a linear topography. We consider the effect of a more general topography in the next section.

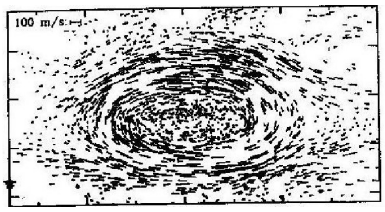


Observation (Voyager)

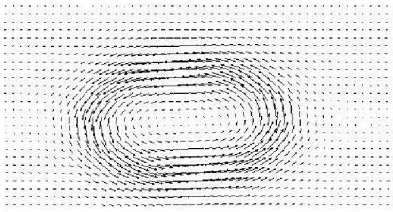

Statistical Equilibrium

Figure 5. Left: the observed velocity field is from Voyager spacecraft data, from Dowling and Ingersoll (1988) ; the length of each line is proportional to the velocity at that point. Note the strong jet structure of width of order $R$, the Rossby deformation radius. Right: the velocity field for the statistical equilibrium model of the Great Red Spot. The actual values of the jet maximum velocity, jet width, vortex width and length fit with the observed ones. The jet is interpreted as the interface between two phases; each of them corresponds to a different mixing level of the potential vorticity. The jet shape obeys a minimal length variational problem (an isoperimetrical problem) balanced by the effect of the deep layer shear.

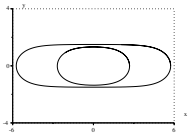

Statistical Equilibria

Great Red Spot and White Oval BC

A Brown Barge

Figure 6. Left panel: typical vortex shapes obtained from the isoperimetrical problem (curvature radius equation (12)), for two different values of the parameters (arbitrary units). The characteristic properties of Jupiter's vortex shapes (very elongated, reaching extremal latitude $y_m$ where the curvature radius is extremely large) are well reproduced by these results. Central panel: the Great Red Spot and one of the White Ovals. Right panel: one of the Brown Barge cyclones of Jupiter's north atmosphere. Note the very peculiar cigar shape of this vortex, in agreement with statistical mechanics predictions (left panel)..

### 3.3.1. *Determination of the vortex shape: the typical elongated shape of Jupiter's features*

In order to determine the effect of topography on the jet shape, we consider again the variational problem (13). We note that the topography $\eta_d = Rh$ has been rescaled by $R$ in the term $Rh(y)\phi$ appearing in the variational problem. This corresponds to a regime where the effect of the

topography is of the same order as the effect of the jet free energy. Two other regimes exist: one for which topography would have a negligible impact (this would lead to circular vortices, as treated in section 3.2) and another regime where topography would play the dominant role. This last regime may be interesting in some cases, but we do not treat it in this review.

Due to the scaling $Rh\phi$, the topography does not play any role at zeroth order. We thus still conclude that phase separation occurs, with subdomains of areas $A_+$ and $A_-$ fixed by the potential vorticity constraint (see section 3.1.1), separated by jets whose transverse structure is described in section 3.1.3. The jet shape is however given by minimization of the free energy contributions of order $R$. Let us thus compute the first order contribution of the topography term $RH = \int_{\mathcal{D}} \mathrm{d}\mathbf{r}\ (-R\phi h(y))$. For this we use the zeroth order result $\phi = \pm u$. We then obtain $H = -u\int_{A_+} \mathrm{d}\mathbf{r}\, h + u\int_{A_-} \mathrm{d}\mathbf{r}\, h = H_0 - 2u\int_{A_+} \mathrm{d}\mathbf{r}\, h$, where $H_0 \equiv u\int_{\mathcal{D}} \mathrm{d}\mathbf{r}\, h$. We note that $H_0$ does not depend on the jet shape.

Adding the contribution of the topography to the jet free energy (10), we obtain the first order expression for the modified free energy functional

$$\mathcal{F} = RH_0 + R\left(eL - 2u\int_{A_+} \mathrm{d}\mathbf{r}\, h(y)\right), \tag{15}$$

which is valid up to correction of order $e\,(R/r)$ and of order $R^2H$. We recall that the total area $A_+$ is fixed. We see that, in order to minimize the free energy, the new term tends to favor as much as possible the phase $A_+$ with positive values of stream function $\phi = u$ (and then negative values of potential vorticity $q = -u$) to be placed on topography maxima. This effect is balanced by the length minimization.

In order to study in more details the shape of the jet, we look at the critical points of the minimization of (15), with fixed area $A_+$. Recalling that first variations of the length are proportional to the inverse of the curvature radius, we obtain

$$2uRh(y) + \alpha = \frac{eR}{r}, \tag{16}$$

where $\alpha$ is a Lagrange parameter associated with the conservation of the area $A_+$. This relates the vortex shape to the topography and parameters $u$ and $e$. From this equation, one can write the equations for $X$ and $Y$, the coordinates of the jet curve. These equations derive from a Hamiltonian, and a detailed analysis allows to specify the initial conditions leading to

closed curves and thus to numerically compute the vortex shape (Bouchet and Sommeria, 2002).

Figure 6 compares the numerically obtained vortex shapes, with the Jovian ones. This shows that the solution to equation (16) has the typical elongated shape of Jovian vortices, as clearly illustrated by the peculiar cigar shape of Brown Barges, which are cyclones of Jupiter's north troposphere. We thus conclude that statistical mechanics and the associated Van-Der-Waals Cahn Hilliard functional with topography explain well the shape of Jovian vortices.

Figure 7 shows a phase diagram for the statistical equilibria, with Jupiter like topography and Rossby deformation radius. This illustrates the power of statistical mechanics: with only few parameters characterizing statistical equilibria (here the energy $E$ and a parameter related to the asymmetry between positive and negative potential vorticity $B$), we are able to reproduce all the features of Jupiter's troposphere, from circular white ovals, to the GRS and cigar shaped Brown Barges. The reduction of the complexity of turbulent flow to only a few order parameters is the main interest and achievement of a statistical mechanics theory.

Moreover, as seen on figure 7, statistical mechanics predicts a phase transition from vortices towards straight jets. The concept of phase transition is an essential one in complex systems, as the qualitative physical properties of the system drastically change at a given value of the control parameters.

### 3.3.2. *Quantitative comparisons with Jupiter's Great Red Spot*

In the preceding section, we have made a rapid description of the effect of a topography to first order phase transitions. We have obtained and compared the vortex shape with Jupiter's vortices. A much more detailed treatment of the applications to Jupiter and to the Great Red Spot can be found in Bouchet and Sommeria (2002); Bouchet and Dumont (2003). The theory can be extended in order to describe the small shear outside of the spot (first order effect on $\phi$ outside of the interface), on the Great Red Spot zonal velocity with respect to the ambient shear, on the typical latitudinal extension of these vortices. A more detailed description of physical considerations on the relations between potential vorticity distribution and forcing is also provided in Bouchet and Sommeria (2002); Bouchet and Dumont (2003).

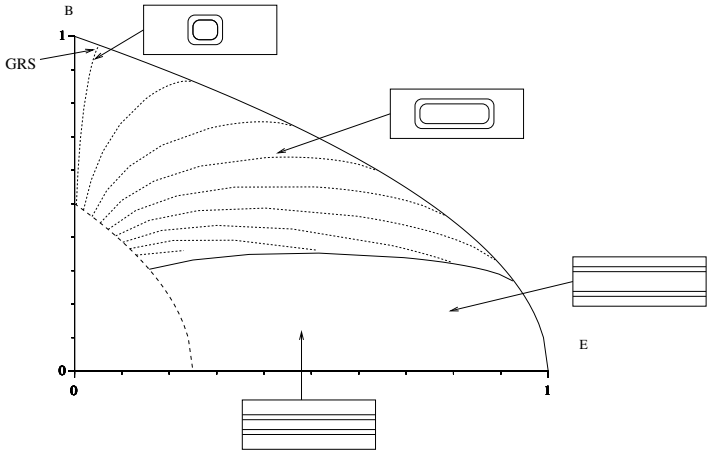


Figure 7. Phase diagram of the statistical equilibrium states versus the energy $E$ and a parameter related to the asymmetry between positive and negative potential vorticity $B$, with a quadratic topography. The inner solid line corresponds to a phase transition, between vortex and straight jet solutions. The dash line corresponds to the limit of validity of the small deformation radius hypothesis. The dot lines are constant vortex aspect ratio lines with values 2,10,20,30,40,50,70,80 respectively. We have represented only solutions for which anticyclonic potential vorticity dominate ($B > 0$). The opposite situation may be recovered by symmetry. For a more detailed discussion of this figure, the precise relation between $E$, $B$ and the results presented in this lecture, please see Bouchet Dumont.

### 3.4. *Application to ocean rings*

Application of equilibrium statistical mechanics to the description of oceanic flows is a long-standing problem, starting with the work of Salmon–Holloway–Hendershott in the framework of energy-enstrophy theory (Salmon *et al.*, 1976).

Another attempt to apply equilibrium statistical mechanics to oceanic flows had been performed by Dibattista and Majda (2000); Dibattista *et al.* (2002) in the framework of the Heton model of Hogg and Stommel (1985) for the self-organization phenomena following deep convection events, by numerically computing statistical equilibrium states of a two-layer quasi-geostrophic model.

None of these previous approaches have explained the ubiquity of oceanic rings. We show in the following that such rings can actually be understood as statistical equilibria by similar arguments that explain the formation of Jovian vortices (see Venaille and Bouchet (2011a) for more

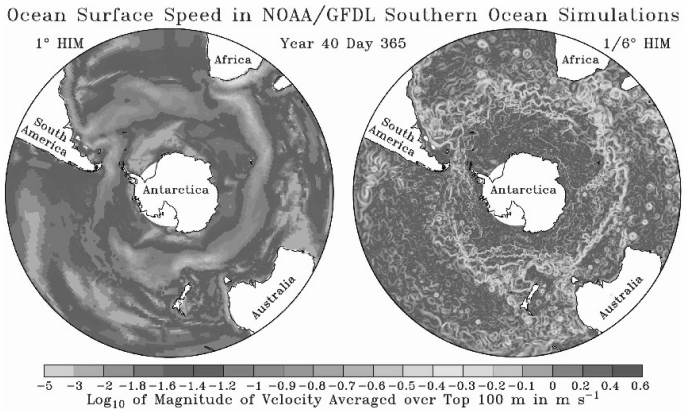


Figure 8. Snapshot of surface velocity field from a comprehensive numerical simulation of the southern Oceans (Hallberg et all 2006). Left: coarse resolution, the effect of mesoscale eddies ($\sim 100km$) is parameterized. Right: higher resolution, without parameterization of mesoscale eddies. Note the formation of large scale coherent structure in the high resolution simulation: there is either strong and thin eastward jets or rings of diameter $\sim 200\ km$. Typical velocity and width of jets (be it eastward or around the rings) are respectively $\sim 1\ m.s^{-1}$ and $\sim 20\ km$. The give a statistical mechanics explanation and model for these rings.

details).

### 3.4.1. *Rings in the oceans*

The ocean has long been recognized as a sea of eddies. This has been first inferred from *in situ* data by Gill, Green and Simmons in the early 1970s (Gill *et al.*, 1974). During the last two decades, the concomitant development of altimetry and realistic ocean modeling has made possible a quantitative description of those eddies. The most striking observation is probably their organization into westward propagating rings of diameters ($L_e \sim 200\ km$), as for instance seen in figure 8. In that respect, they look like small Jovian Great Red Spots.

Those eddies plays a crucial role for the general ocean circulation and its energy cycle, since their total energy is one order of magnitude above the kinetic energy of the mean flow.

Those rings are mostly located around western boundary currents, which are regions characterized by strong baroclinic instabilities[f], such as

[f]When the mean flow present a sufficiently strong vertical shear, baroclinic instabilities

the Gulf Stream, the Kuroshio, the Aghulas currents below South Africa or the confluence region of the Argentinian basin, as seen on figures 8 and 11. The rings can also propagate far away from the regions where they are created.

Most of those rings have a baroclinic structure, i.e. a velocity field intensified in the upper layer ($H \sim 1\ km$) of the oceans. This baroclinic structure suggest that the 1.5 layer quasi-geostrophic model introduced in the previous sections is relevant to this problem. The horizontal scale of the rings ($L_e \sim 200\ km$) are larger than the width $R \sim 50\ km$ of the surrounding jet, of typical velocities $U = 1\ m.s^{-1}$.

The organization of those eddies into coherent rings can be understood by the same statistical mechanics arguments that have just been presented in the case of Jupiter's Great Red Spot. The rings correspond to one phase containing most of the potential vorticity extracted from the mean flow by baroclinic instability, while the surrounding quiescent flow corresponds to the other phase. This statistical mechanics approach, the only one to our knowledge to describe the formation of large scale coherent structures, might then be extremely fruitful to account for the formation of such rings. It remains an important open question concerning the criteria that select the size of such coherent structures. This is an ongoing subject of investigation.

### 3.4.2. *The westward drift of the rings*

In this section, we consider the consequences of the beta effect (see section 2.1), which corresponds to linear topography $\eta_d = \beta y$ in (2). We prove that this term can be easily handled and that it actually explains the westward drift of oceanic rings with respect to the mean surrounding flow.

We consider the quasi-geostrophic equations on a domain which is invariant upon a translation along the $x$ direction (either an infinite or a periodic channel, for instance). Then the quasi-geostrophic equations are invariant over a Galilean transformation in the $x$ direction. We consider the transformation $\mathbf{v}' = \mathbf{v} + V\mathbf{e}_x$, where $\mathbf{v}$ is the velocity in the original frame of reference and $\mathbf{v}'$ is the velocity in the new Galilean frame of reference.

From the relation $\mathbf{v} = \mathbf{e}_z \wedge \nabla\psi$, we obtain the transformation law for $\psi$: $\psi' = \psi - Vy$ and from the expression $q = \Delta\psi - \psi/R^2 + \beta y$ (2) we obtain

release part of the available potential energy associated with this mean flow, which is generally assumed to be maintained by a large scale, low frequency forcing mechanism such as surface wind stress or heating (Vallis, 2006)

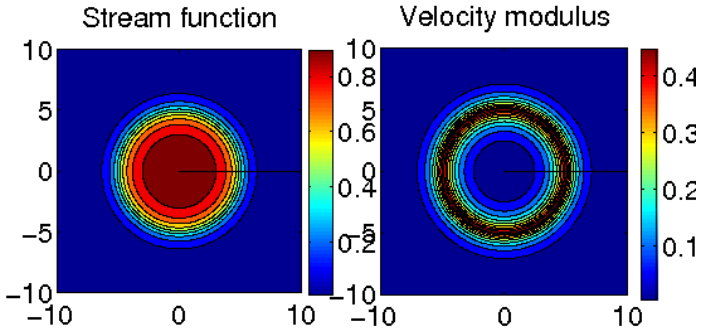


Figure 9. Vortex statistical equilibria in the quasi-geostrophic model. It is a circular patch of (homogenized) potential vorticity in a background of homogenized potential vorticity, with two different mixing values. The velocity field (right panel) has a very clear ring structure, similarly to the Gulf-Stream rings and to many other ocean vortices. The width of the jet surrounding the ring has the order of magnitude of the Rossby radius of deformation $R$.

the transformation law for $q$: $q' = q + Vy/R^2$. Thus the expression for the potential vorticity in the new reference frame is

$$q = \Delta\psi - \frac{\psi}{R^2} + \left(\beta + \frac{V}{R^2}\right) y.$$

From this last expression, we see that a change of Galilean reference frame translates as a beta effect in the potential vorticity. Moreover, in a reference frame moving at velocity $-\beta R^2 \mathbf{e}_x$, the $\beta$ effect is exactly canceled out.

From this remark, we conclude that taking into account the beta effect, the equilibrium structures should be the one described by the minimization of the Van-Der-Waals Cahn Hilliard variational problem, but moving at a constant westward speed $V = \beta R^2$. A more rigorous treatment of the statistical mechanics for the quasi-geostrophic model with translational invariance would require to take into account an additional conserved quantity, the linear momentum, which would lead to the same conclusion: statistical equilibria are rings with a constant westward speed $V = \beta R^2$. See also Venaille and Bouchet (2011a) for more details and discussions on the physical consequences of this additional constraint.

This drift is actually observed for the oceanic rings, see for instance figure 10.

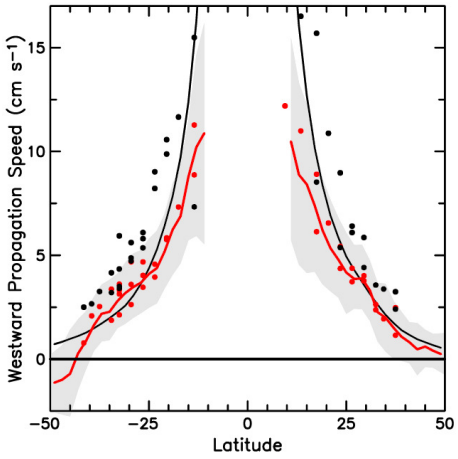


Figure 10. Altimetry observation of the westward drift of oceanic eddies (including rings) (Chelton et al, 2007), figure 4. The red line is the zonal average (along a latitude circle) of the propagation speeds of all eddies with life time greater than 12 weeks. The black line represents the velocity $\beta R^2$ where $\beta$ is the meridional gradient of the Coriolis parameter and $R$ the first baroclinic Rossby radius of deformation. This eddy propagation speed is a prediction of statistical mechanics

## 4. Are the Gulf-Stream and the Kuroshio currents close to statistical equilibria?

In section 3.4, we have discussed applications of statistical mechanics ideas to the description of ocean vortices, like the Gulf-Stream rings. We have also mentioned that statistical equilibria, starting from the Van-Der-Waals Cahn Hilliard functional (13), may model physical situations where strong jets, with a width of order $R$, bound domains of nearly constant potential vorticity.

This is actually the case of the Gulf Stream in the North Atlantic ocean or of the Kuroshio extension in the North Pacific ocean. This can be inferred from observations, or this is observed in high resolution numerical simulations of idealized wind driven mid-latitude ocean, see for instance figure 12 (see Berloff *et al.* (2007) for more details).

It is thus very tempting to interpret the Gulf Stream and the Kuroshio as interfaces between two phases corresponding to different levels of potential vorticity mixing, just like the Great Red Spot and ocean rings in the previous section. The aim of this chapter is to answer this natural question: are the Gulf-Stream and Kuroshio currents close to statistical equilibria?

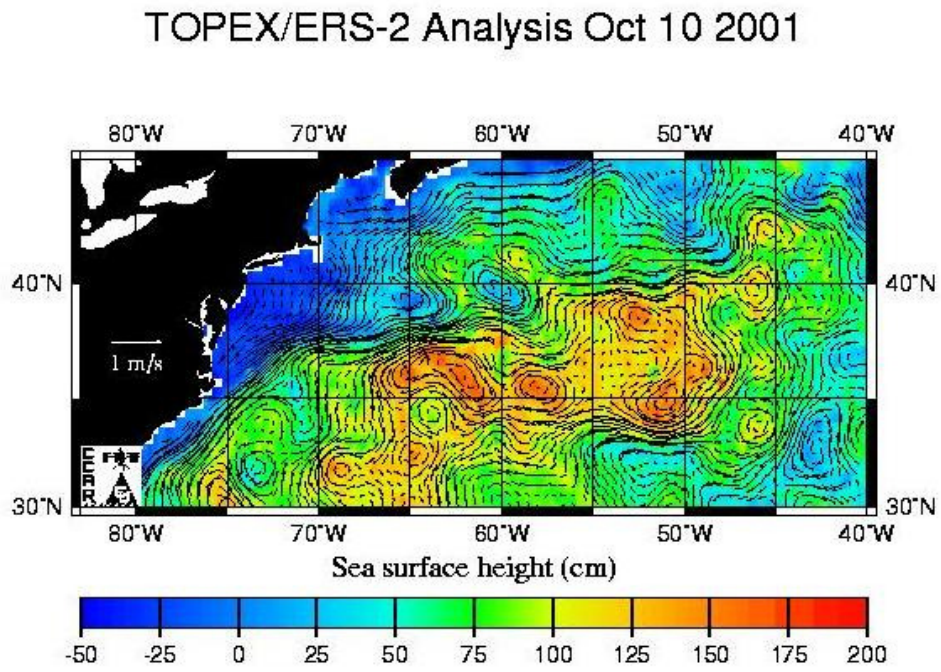


Figure 11. Observation of the sea surface height of the north Atlantic ocean (Gulf Stream area) from altimetry (Topex-Poseidon). For geophysical flows, the surface velocity field can be inferred from the see surface height (SSH): strong gradient of SSH are related to strong jets. The Gulf stream appears as a robust eastward jet (in presence of meanders), flowing along the east coast of north America and then detaching the coast to enter the Atlantic ocean, with an extension $L \sim 2000\ km$. The jet is surrounded by numerous westward propagating rings of typical diameters $L \sim 200\ km$. Typical velocities and widths of both the Gulf Stream and its rings jets are respectively $1\ m.s^{-1}$ and $50\ km$, corresponding to a Reynolds number $Re \sim 10^{11}$. Such rings can be understood as local statistical equilibria, and strong eastward jets like the Gulf Stream and obtained as marginally unstable statistical equilibria in simple academic models (see subsections 3.4-4).

More precisely, we address the following problem: is it possible to find a class of statistical equilibria with a strong mid-basin eastward jet similar to the Gulf Stream of the Kuroshio, in a closed domain? The 1-1/2 layer quasi-geostrophic model (see section 2.1) is the simplest model taking into account density stratification for mid-latitude ocean circulation in the upper first $1000\,m$ (Pedlosky, 1998; Vallis, 2006). We analyze therefore the class of statistical equilibria which are minima of the Van-Der-Waals Cahn Hilliard

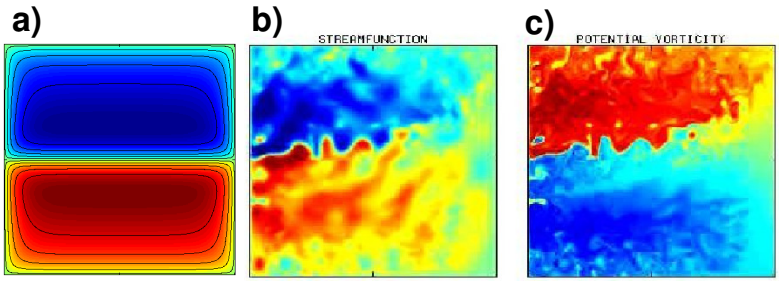


Figure 12. b) and c) represent respectively a snapshot of the streamfunction and potential vorticity (red: positive values; blue: negative values) in the upper layer of a three layers quasi-geostrophic model in a closed domain, representing a mid-latitude oceanic basin, in presence of wind forcing. Both figures are taken from numerical simulations by P. Berloff. a) Streamfunction predicted by statistical mechanics, see section 4 for further details. Even in an out-equilibrium situation like this one, the equilibrium statistical mechanics predicts correctly the overall qualitative structure of the flow.

variational problem (13), as explained in section 3.2. We ask whether it exists solutions to

$$\left\{ \begin{array}{c} F = \min \left\{ \mathcal{F}\left[\phi\right] \ | \ A\left[\phi\right] = -B \right\} \\ \text{with} \ \ \mathcal{F} = \int_{\mathcal{D}} d\mathbf{r} \left[ \frac{R^2 (\nabla \phi)^2}{2} + f\left(\phi\right) - R\tilde{\beta} y \phi \right] \ \ \text{and} \ \ \mathcal{A}\left[\phi\right] = \int_{\mathcal{D}} d\mathbf{r}\, \phi \end{array} \right. \tag{17}$$

in a bounded domain (let say a rectangular basin) with strong mid-basin eastward jets. At the domain boundary, we fix $\phi = 0$ (which using $\phi = R^2 \psi$ turns out to be an impermeability condition). We note that the understanding of the following discussion requires the reading of sections 4.1 to 4.3.

The term $R\tilde{\beta} y$ is an effective topography including the beta effect and the effect of a deep zonal flow (see section 2.1). Its significance and effects will be discussed in section 5.2. As in the previous section, we consider the limit $R \ll L$ and assume $f$ be a double well function.

As discussed in chapter 3.1, with these hypothesis, there is phase separation in two subdomains with two different levels of potential vorticity mixing. These domains are bounded by interfaces (jets) of width $R$. In view of the applications to mid-basin ocean jets, we assume that the area $A_+$ occupied by the value $\phi = u$ is half of the total area of the domain (this amounts to fix the total potential vorticity $\Gamma_1$). The question is to determine the position and shape of this interface. The main difference with the cases treated in subsection 3.1 is due to the effect of boundaries and of the linear effective topography $R\tilde{\beta} y$.

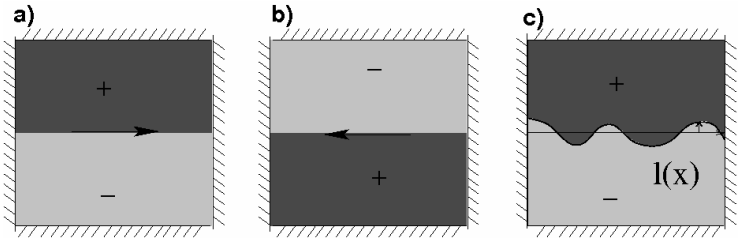


Figure 13. a) Eastward jet: the interface is zonal, with positive potential vorticity $q = u$ on the northern part of the domain. b) Westward jet: the interface is zonal, with negative potential vorticity $q = -u$ in the northern part of the domain. c) Perturbation of the interface for the eastward jet configuration, to determine when this solution is a local equilibrium (see subsection 4.2). Without topography, both (a) and (b) are entropy maxima. With positive beta effect (b) is the global entropy maximum; with negative beta effect (a) is the global entropy maximum.

### 4.1. *Eastward jets are statistical equilibria of the quasi-geostrophic model without topography*

The value $\phi = \pm u$ for the two coexisting phases is not compatible with the boundary condition $\phi = 0$. As a consequence, there exists a boundary jet (or boundary layer) in order to match a uniform phase $\phi = \pm u$ to the boundary conditions. Just like inner jets, treated in section 3, these jets contribute to the first order free energy, which gives the jet position and shape. We now treat the effect of boundary layer for the case $h = 0$ ($\widetilde{\beta} = 0$ in this case). As explained in section 3.1.3, the jet free energy is the only contribution to the total free energy.

We first quantify the unit length free energy, $F_b$, for the boundary jets. Following the reasoning of section 3.1.3, we have

$$F_b = \min \left\{ \int d\zeta \, \left[ \frac{R^2}{2} \frac{d^2\phi}{d\zeta^2} + f(\phi) \right] \right\}.$$

This expression is the same as (8), the only difference is the different boundary conditions: it was $\phi \to_{\zeta \to +\infty} u$ and $\phi \to_{\zeta \to -\infty} -u$, it is now $\phi \to_{\zeta \to +\infty} u$ and $\phi\,(0) = 0$. Because $f$ is even, one easily see that a boundary jet is nothing else than half of a interior domain jet. Then

$$F_b = \frac{1}{2} F_{int} = \frac{e}{2} R,$$

where $F_{int}$ and $e$ are the unit length free energies for the interior jets, as defined in section 3.1.3. By symmetry, a boundary jet matching the value

$\phi = -u$ to $\phi = 0$ gives the same contribution[g]. Finally, the first order free energy is given by

$$\mathcal{F} = eR\left(L + \frac{L_b}{2}\right),$$

where $L_b$ is the boundary length. Because the boundary length $L_b$ is a fixed quantity, the free energy minimization amounts to the minimization of the interior jet length. The interior jet position and shape is thus given by the minimization of the interior jet length with fixed area $A_+$. We recall that the solutions to this variational problem are interior jets which are either straight lines or circles (see section 3.1.3).

In order to simplify the discussion, we consider the case of a rectangular domain of aspect ratio $\tau = L_x/L_y$. Generalization to an arbitrary closed domain could also be discussed. We recall that the two phases occupy the same area $A_+ = A_- = \frac{1}{2}L_xL_y$. We consider three possible interface configurations with straight or circular jets:

(1) the zonal jet configuration (jet along the $x$ axis) with $L = L_x$,
(2) the meridional jet configuration (jet along the $y$ axis with $L = L_y$,
(3) and an interior circular vortex, with $L = 2\sqrt{\pi A_+} = \sqrt{2\pi L_x L_y}$ .

The minimization of $L$ for these three configurations shows that the zonal jet is a global minimum if and only if $\tau < 1$. The criterion for the zonal jet to be a global RSM equilibrium state is then $L_x < L_y$. We have thus found zonal jet as statistical equilibria in the case $h = 0$.

An essential point is that both the Kuroshio and the Gulf Stream are flowing eastward (from west to east). From the relation $\mathbf{v} = \mathbf{e}_z \times \nabla\psi$, we see that the jet flows eastward ($v_x > 0$) when $\partial_y\psi < 0$. Recalling that $\phi = R^2\psi$, the previous condition means that the negative phase $\phi = -u$ has to be on the northern part of the domain, and the phase $\phi = u$ on the southern part. From (2), we see that this corresponds to a phase with positive potential vorticity $q = u$ on the northern sub-domains and negative potential vorticity $q = -u$ on the southern sub-domain, as illustrated in the panel (a) of figure (13).

Looking at the variational problems (17), it is clear that in the case $\widetilde{\beta} = 0$, the minimization of $\phi$ is invariant over the symmetry$\phi \to -\phi$. Then

[g]We have treated the symmetric case when $f$ is even. The asymmetric case could be also easily treated

solutions with eastward or westward jets are completely equivalent. Actually there are two equivalent solutions for each of the case 1, 2 and 3 above. However, adding a beta effect $h = R\widetilde{\beta}y$ will break this symmetry. This is the subject of next section.

We conclude that in a closed domain with aspect ratio $L_x/L_y < 1$, without topography, equilibrium states exist with an eastward jet at the center of the domain, recirculating jets along the domain boundary and a quiescent interior. For $L_x/L_y > 1$, these solutions become metastable states (local entropy maximum). This equilibrium is degenerated, since the symmetric solution with a westward jet is always possible.

### 4.2. *Addition of a topography*

For ocean dynamics, the beta effect plays a crucial role. Let us now consider the case where the topography is $\eta_d = \beta y + \frac{\psi_d}{R^2}$. The first contribution comes from the beta-effect (the variation of the Coriolis parameter with latitude). The second contribution is a permanent deviation of the interface between the upper layer and the lower layer. For simplicity, we consider the case where this permanent interface elevation is driven by a constant zonal flow in the lower layer: $\psi_d = -U_d y$ , which gives $\eta_d = \left(\beta - \frac{U_d}{R^2}\right) y = R\widetilde{\beta}y$. Then the combined effect of a deep constant zonal flow and of the variation of the Coriolis parameter with latitude is an effective linear beta effect.

In the definition of $\widetilde{\beta}$ above, we use a rescaling with $R$. This choice is considered in order to treat the case where the contribution of the effective beta effect appears at the same order as the jet length contribution. This allows to easily study how the beta effect breaks the symmetry $\phi \to -\phi$ between eastward and westward jets. Following the arguments of section 3.3.1, we minimize

$$\mathcal{F} = RH_0 + R\left(eL - 2u\int_{A_+} \mathrm{d}\mathbf{r}\,\tilde{\beta}y\right), \tag{18}$$

(see equation (15)), with a fixed area $A_+$. The jet position is a critical point of this functional: $e/r - 2u\tilde{\beta}y_{jet} = \alpha$ (see equation (16)), where $\alpha$ is a Lagrange parameter and $y_{jet}$ the latitude of the jet. We conclude that zonal jets (curves with constant $y_{jet}$ and $r = +\infty$) are solutions to this equation for $\alpha = -2uR\tilde{\beta}y_{jet}$. Eastward and westward jets described in the previous section are still critical points of entropy maximization.

#### 4.2.1. *With a negative effective beta effect, eastward jets are statistical equilibria*

We first consider the case $\widetilde{\beta} < 0$. This occurs when the zonal flow in the lower layer is eastward and sufficiently strong ($U_d > R^2\beta$). If we compute the first order free energy (18) for both the eastward and the westward mid-latitude jet, it is easy to see that in order to minimize $\mathcal{F}$, the domain $A_+$ has to be located at the lower latitudes: taking $y = 0$ at the interface, the term $-2u \int_{A_+} d^2\mathbf{r}\, \tilde{\beta} y = u\tilde{\beta} L_x L_y/4$ gives a negative contribution when the phase with $\phi = u$ (and $q = -u$) is on the southern part of the domain ($A_+ = (0, L_x) \times (-\frac{L_y}{2}, 0)$). This term would give the opposite contribution if the phase $\phi = u$ would occupy the northern part of the domain. Thus the statistical equilibria is the one with negative streamfunction $\phi$ (corresponding to positive potential vorticity $q$) on the northern part of the domain. As discussed in the end of section 4.1 and illustrated on figure 13, panel (b), this is the case of an eastward jet.

Thus, we conclude that taking into account an effective negative beta-effect term at first order breaks the westward-eastward jet symmetry. When $\widetilde{\beta} < 0$, statistical equilibria are flows with mid-basin eastward jets.

#### 4.2.2. *With a positive effective beta effect, westward jets are statistical equilibria*

Let us now assume that the effective beta coefficient is positive. This is the case when $U_d < R^2\beta$, i.e. when the lower layer is either flowing westward, or eastward with a sufficiently low velocity. The argument of the previous paragraph can then be used to show that the statistical equilibrium is the solution presenting a westward jet.

#### 4.2.3. *With a sufficiently small effective beta coefficient, eastward jets are local statistical equilibria*

We have just proved that mid-basin eastward jets are not global equilibria in the case of positive effective beta effect. They are however critical points of entropy maximization. They still could be local entropy maxima. We now consider this question: are mid-basin strong eastward jets local equilibria for a positive effective beta coefficient? In order to answer, we perturb the interface between the two phases, while keeping constant the area they occupy, and compute the free energy perturbation.

The unperturbed interface equation is $y = 0$, the perturbed one is $y = l(x)$, see figure 13. Qualitatively, the contributions to the free energy $\mathcal{F}$ (18), of the jet on one hand and of the topography on the other hand, are competing with each other. Any perturbation increases the jet length $L = \int dx \ \sqrt{1 + \left(\frac{dl}{dx}\right)^2}$ and then increases the second term in equation (18) by $\delta\mathcal{F}_1 = Re \int dx \ (dl/dx)^2$. Any perturbation decreases the third term in equation (18) by $\delta\mathcal{F}_2 = -2Ru\tilde{\beta} \int dx \ l^2$.

We suppose that $l = l_k \sin \frac{k\pi}{L_x} x$ where $k \geq 1$ is an integer. Then

$$\delta\mathcal{F} = \delta\mathcal{F}_1 + \delta\mathcal{F}_2 = -2u\tilde{\beta} + e\left(\frac{k\pi}{L_x}\right)^2 .$$

Because we minimize $\mathcal{F}$, we want to know if any perturbation leads to positive variations of the free energy. The most unfavorable case is for the smallest value of $k^2$, i.e. $k^2 = 1$. Then we conclude that eastward jets are local entropy maxima when

$$\widetilde{\beta} < \widetilde{\beta}_{cr} = \frac{1}{2}\frac{e}{u}\frac{\pi^2}{L_x^2} \ .$$

We thus conclude that eastward zonal jets are local equilibria for sufficiently small values of $\widetilde{\beta}$.

The previous result can also be interpreted in terms of the domain geometry, for a fixed value of $\widetilde{\beta}$. Eastward jets are local entropy maxima if

$$L_x < L_{x,cr} = \pi\sqrt{\frac{e}{2u\widetilde{\beta}_{cr}}}.$$

Let us evaluate an order of magnitude for $L_{x,cr}$ for the ocean case, first assuming there is no deep flow ($U_d = 0$). Then $R\tilde{\beta}$ is the real coefficient of the beta plane approximation. Remembering that a typical velocity of the jet is $U \sim uR$, and using $e \sim u^2$ (see Venaille and Bouchet (2011a) for more details). Then $L_{x,cr} \approx \pi\sqrt{\frac{U}{\beta_{cr}}}$. This length is proportional to the Rhine's' scale of geophysical fluid dynamics (Vallis, 2006). For jets like the Gulf Stream, typical jet velocity is 1 $m.s^{-1}$ and $\beta \sim 10^{-11}$ $m^{-1}.s^{-1}$ at mid-latitude. Then $L_{cr} \sim 300$ $km$. This length is much smaller than the typical zonal extension of the inertial part of the Kuroshio or Gulf Stream currents. We thus conclude that in a model with a quiescent lower layer and the beta plane approximation, currents like the Gulf Stream or the Kuroshio are not statistical equilibria, and they are not neither close to local statistical equilibria.

Taking the oceanic parameters ($\beta = 10^{-11}\ m^{-1}s^{-1}$, $R \sim 50\ km$), we can estimate the critical eastward velocity in the lower layer $U_{d,cr} = 5\ cm\ s^{-1}$ above which the strong eastward jet in the upper layer is a statistical equilibria. It is difficult to make further conclusions about real mid-latitude jets; we conjecture that their are marginally stable. This hypothesis of marginal stability is in agreement with the observed instabilities of the Gulf-Stream and Kuroshio current, but overall stability of the global structure of the flow. A further discussion of these points will be the object of future works.

In all of the preceding considerations, we have assumed that the term $R\widetilde{\beta}$ was of order $R$ in dimensionless units. This is self-consistent to compute the unstable states. To show that a solution is effectively a statistical equilibria when $R\widetilde{\beta}$ in of order one, one has to use much less straightforward considerations than in the preceding paragraphs, but the conclusions would be exactly the same.

### 4.3. *Conclusion*

We have shown that when there is a sufficiently strong eastward flow in the deep layer (i.e. when $U_d > U_{d,cr}$ with $U_{d,cr} = R^2\beta_{cr}$), ocean mid-latitude eastward jets are statistical equilibria, even in presence of a beta plane. When the flow in the deep layer is lower than the critical value $U_{d,cr}$ but still almost compensate the beta plane ($0 < \beta - \frac{U_d}{R^2} < \frac{1}{2}\frac{e}{u}\frac{\pi^2}{L_x^2}R$), the solutions with the eastward jets are local equilibria (metastable states). When $\beta - \frac{U_d}{R^2} > \frac{1}{2}\frac{e}{u}\frac{\pi^2}{L_x^2}R$ the solution with an eastward jet are unstable.

We have also concluded that the inertial part of the real Gulf-Stream or of the Kuroshio extension are likely to be marginally stable from a statistical mechanics point of view.

The statistical equilibria that we have described in this section have a flow structure that differs notably from the celebrated Fofonoff solution (Fofonoff, 1954).

The Fofonoff solution is a stationary state of the quasi-geostrophic equations (1-2) on a beta plane ($\eta_d = \beta y$) obtained by assuming a linear relationship between potential vorticity and streamfunction ($q = a\psi$), in the limit $a + R^{-2} \gg L^{-2}$, where $L$ is the domain size. In this limit, the Laplacian term in (2) is negligible in the domain bulk. Then $\psi \approx \beta/(a+R^{-2})y$, which corresponds to a weak westward flow, as illustrated figure 14. Strong recirculating eastward jets occur at northern and southern boundaries, where

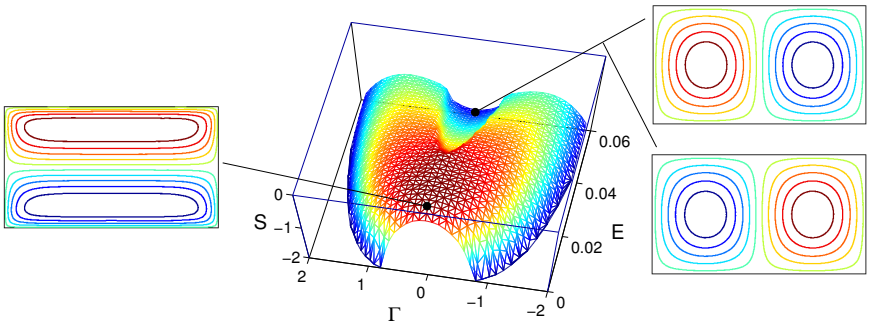


Figure 14. Phase diagrams of RSM statistical equilibrium states of the 1.5 layer quasi-geostrophic model, characterized by a linear $q - \psi$ relationship, in a rectangular domain elongated in the $x$ direction. $S(E, \Gamma)$ is the equilibrium entropy, $E$ is the energy and $\Gamma$ the circulation. Low energy states are the celebrated Fofonoff solutions, presenting a weak westward flow in the domain bulk. High energy states have a very different structure (a dipole). Please note that at high energy the entropy is non-concave. This is related to ensemble inequivalence, which explain why such states were not computed in previous studies (Please see Venaille and Bouchet, 2009, for more details).

the Laplacian term is no more negligible.

The original work of Fofonoff was carried independently from statistical mechanics considerations. The linear $q - \psi$ relationship was chosen as a starting point to compute analytically the flow structure. Because both the Salmon–Holloway–Hendershott statistical theory (Salmon *et al.*, 1976) and the Bretherton–Haidvoguel minimum enstrophy principle (Bretherton and Haidvogel, 1976) did predict a linear relationship between vorticity and streamfunction, it has been argued that statistical equilibrium theory predicts the emergence of the classical Fofonoff flows, which had effectively been reported in numerical simulations of freely decaying barotropic flows on a beta plane for some range of parameters (Wang and Vallis, 1994).

It is shown in Bouchet (2008) that all those theories are particular cases of the RSM statistical mechanics theory. On the one hand it has been actually proven that the classical Fofonoff solutions are indeed RSM statistical equilibria in the limit of low energies (Venaille and Bouchet, 2011b). On the other hand, as illustrated by the results of this section, there exists a much richer variety of RSM equilibrium states than the sole classical Fofonoff solution. Even in the case of a linear $q - \psi$ relation, high energy statistical equilibrium states are characterized by a flow structure that differs notably from the original Fofonoff solution, as illustrated figure 14. These high energy states correspond actually to the RSM equilibrium states of the Euler

equation, originally computed by Chavanis and Sommeria (1996). The transition from classical Fofonoff solutions to those high energy states has been related the the occurrence of ensemble inequivalence (Venaille and Bouchet, 2009). This explains also why such high energy states have not been reported in earlier studies, where computations were always performed in the (unconstrained) canonical ensemble, see Venaille and Bouchet (2011b) for more details.

The early work of Fofonoff and the equilibrium statistical mechanics of geophysical flows presented in this review are often referred to as the inertial approach of oceanic circulation, meaning that the effect of the forcing and the dissipation are neglected.

Ocean dynamics is actually much influenced by the forcing and the dissipation. For instance the mass flux of a current like the Gulf Stream is mainly explained by the Sverdrup transport. Indeed in the bulk of the ocean, a balance between wind stress forcing and beta effect (the Sverdrup balance) lead to a meridional global mass flux (for instance toward the south on the southern part of the Atlantic ocean. This fluxes is then oriented westward and explain a large part of the Gulf Stream mass transport. This mechanism is at the base of the classical theories for ocean dynamics, see e.g. Pedlosky (1998). Because it is not an conservative process, the inertial approach does not take this essential aspect into account. Conversely, the traditional theory explains the Sverdrup transport, the westward intensification and boundary current, but gives no clear explanation of the structure of the inertial part of the current: the strongly eastward jets.

Each of the classical ocean theory or of the equilibrium statistical mechanics point of view give an incomplete picture, and complement each other. Another interesting approach consider the dynamics from the point of view of bifurcation theory when the Reynolds number (or some other controlled parameters) are increased. These three types of approaches seem complimentary and we hope they may be combined in the future in a more comprehensive non-equilibrium theory.

## 5. The vertical structure of geostrophic turbulence

In the previous sections, we assumed that the dynamics took place in an upper active layer above a lower layer at rest. Vertical energy transfers were therefore neglected. The vertical structure of the oceanic mesoscale (from 50 to 500 km) is actually a fundamental problem in geophysical fluid dynamics, one that has has been reinvigorated by the need to interpret altimetric

observation of surface velocity fields (Scott and Wang, 2005; Lapeyre, 2009).

It is widely accepted that the energy of oceanic mesoscale currents is mostly injected at the surface of the oceans (Ferrari and Wunsch, 2009). Indeed, the primary source of geostrophic turbulence is mostly baroclinic instability, extracting turbulent energy from the potential energy reservoir set at the basin scale by large scale wind patterns (Gill *et al.*, 1974), and involving surface-intensified unstable modes, see e.g. Smith (2007).

It leads to the following question: what is the vertical structure of a three dimensional quasi-geostrophic flow in the presence of surface forcing ? A first step to tackle this problem is to consider a simpler problem without forcing and dissipation: does an initially surface-intensified flow remain trapped at the surface or does it spread on the vertical ? Here we address this issue in the framework of freely-evolving stratified quasi-geostrophic turbulence, which allows for theoretical analysis with equilibrium statistical mechanics.

We introduce in the next subsection the continuously stratified quasi-geostrophic dynamics, and explain how to compute equilibrium states in a low energy limit.

We examine in a second subsection what are the precise conditions for the oft-cited barotropization process to occur. Barotropization refers to the tendency of a quasi-geostrophic flow to reach a depth-independant flow (Charney, 1971; Rhines, 1977). We study in particular the key role played by the beta effect (the existence of planetary vorticity gradients) in such barotropization processes.

Finally, we show in a third subsection that the formation of bottom trapped-flow in the presence of bottom-topography may be accounted for by statistical mechanics arguments.

### 5.1. *Continuously stratified quasi-geostrophic flows*

Continuously stratified quasi-geostrophic flows take place in three dimensions, but their dynamics is quasi two-dimensional because the non-divergent advecting velocity field has only horizontal components, and can be described by a streamfunction $\psi(x, y, z, t)$. Such flows are stably stratified with a prescribed buoyancy profile $N(z)$ above a topographic anomaly $h_b(x, y)$, and are strongly rotating at a rate $f_0/2$. In the absence of forcing and dissipation, the dynamics is expressed as the advection of potential vorticity $q(x, y, z, t)$ (see e.g. Vallis (2006), section 5.4):

$$\partial_t q + \mathbf{v} \cdot \nabla q = 0 \ , \quad \mathbf{v} = \mathbf{e}_z \times \nabla \psi \tag{19}$$

$$q = \Delta \psi + \frac{\partial}{\partial z} \left( \frac{f_0^2}{N^2} \frac{\partial}{\partial z} \psi \right) + \beta y \ , \tag{20}$$

where $\Delta$ is the horizontal Laplacian, and where we have considered the beta plane approximation (see section 2). The boundary condition at the bottom ($z = -H$, where $H$ is now the averaged ocean depth) is given by

$$\frac{f_0}{N^2} \partial_z \psi \Big|_{z=-H} = -h_b \ , \tag{21}$$

The boundary condition at the surface (defined as $z = 0$, using the rigid lid approximation), is given by the advection of buoyancy

$$\partial_t b_s + \mathbf{v}|_{z=0} \cdot \nabla b_s = 0 \ , \quad \frac{f_0^2}{N^2} \partial_z \psi \Big|_{z=0} = b_s. \tag{22}$$

The upper boundary condition (22) can be formally replaced by the condition of no buoyancy variation ($\partial_z \psi = 0$ at $z = 0$), provided that surface buoyancy anomalies are interpreted as a thin sheet of potential vorticity just below the rigid lid (Bretherton, 1966). For this reason, and without loss of generality, we will consider that $b_s = 0$ in the remainder of this course. In the following we will consider the case of a square doubly-periodic domain $\mathcal{D}$, and we choose to adimensionalize length such that the domain length is $2\pi$, so that the streamfunction is $2\pi$-periodic in the $x, y$ direction.

The dynamics admits similar conservation laws as the one-layer quasi-geostrophic model considered in sections 2-3-4. Dynamical invariants include the total (kinetic plus potential) energy

$$\mathcal{E} = \frac{1}{2} \int_{-H}^{0} \mathrm{d}z \ \int_{\mathcal{D}} \mathrm{d}x\mathrm{d}y \ \left[ (\nabla \psi)^2 + \frac{f_0^2}{N^2} \left( \partial_z \psi \right)^2 \right], \tag{23}$$

and the Casimir functionals $\mathcal{C}_g(z)[q] = \int_{\mathcal{D}} \mathrm{d}x\mathrm{d}y \ g(q)$ where $g$ is any continuous function. These conservation laws have important physical consequences. In particular, there is an inverse energy cascade that leads to the formation of robust, large scale coherent structures filling the domain in which the flow takes place. It is shown in Venaille *et al.* (2012) that the vertical structure of the large scale flow organization resulting from inviscid, freely evolving continuously stratified quasi-geostrophic dynamics can be predicted using equilibrium statistical mechanics. We sum up the main results in the next subsections.

5.1.1. *Equilibrium states characterized by a linear $q - \psi$ relation*

Let us call $E_0 = \mathcal{E}(q_0)$ and $Z_0(z) = (1/2)\int_{\mathcal{D}} \mathrm{d}x\mathrm{d}y\ q_0^2$ the energy and enstrophy, respectively, of the initial condition given by $q_0(x, y, z)$. Using a general result of Bouchet (2008), it is shown in Venaille *et al.* (2012), Appendix 1, that in the *low energy limit*, the calculation of RSM equilibrium states amounts to finding the minimizer $\overline{q}_{min}$ of the "total macroscopic enstrophy"

$$\mathcal{Z}_{cg}^{tot}\left[\overline{q}\right] = \frac{1}{2}\int_{-H}^{0} \mathrm{d}z \int_{\mathcal{D}} \mathrm{d}x\mathrm{d}y\ \frac{\overline{q}^2}{Z_0} \tag{24}$$

among all the fields $\overline{q}$ satisfying the energy constraint

$$\mathcal{E}[\overline{q}] = \frac{1}{2}\int_{\mathcal{D}} \mathrm{d}x\mathrm{d}y\ f_0 h_b \psi|_{z=-H} - \frac{1}{2}\int_{\mathcal{D}} \mathrm{d}x\mathrm{d}y \int_{-H}^{0} \mathrm{d}z\ (\overline{q} - \beta y)\,\psi = E_0, \tag{25}$$

The variational problem (24-25) can be seen as a generalization to the stratified case of the phenomenological minimum enstrophy principle of Bretherton and Haidvogel (1976).

Critical states of the variational problem (24-25) are computed by introducing Lagrange multiplier $\beta_t$ associated with the energy constraint, and by solving $\delta\mathcal{Z}_{cg}^{total} + \beta_t \delta\mathcal{E} = 0$,, leading to the linear relation $\overline{q} = \beta_t Z_0 \psi$. The next step is to find which of these critical states are actual minimizers of the macroscopic enstrophy for a given energy. We perform these computations in various cases of geophysical interest in the following subsections.

## 5.2. *The presence of a beta plane favors barotropization*

5.2.1. *Equilibrium states without topography and without beta effect*

We consider here the case $h_b = 0$ and $\beta = 0$. Injecting $\overline{q} = \beta_t Z_0 \psi$ in (20) and projecting on Fourier modes yields

$$\frac{\partial}{\partial z}\left(\frac{f_0^2}{N^2}\frac{\partial}{\partial z}\widehat{\psi}_{k,l}\right) = \left(\beta_t Z_0 + K^2\right)\widehat{\psi}_{k,l}\ , \tag{26}$$

with

$$\partial_z \widehat{\psi}_{k,l}|_{z=0,-H} = 0, \quad K^2 = k^2 + l^2, \quad \psi = \sum_{k,l} \widehat{\psi}_{k,l} \exp\left(2i\pi\left(kx + ly\right)\right).$$

We see that each critical point is characterized by a given wavenumber modulus $K$. Its vertical structure and the corresponding value of $\beta_t$ must be

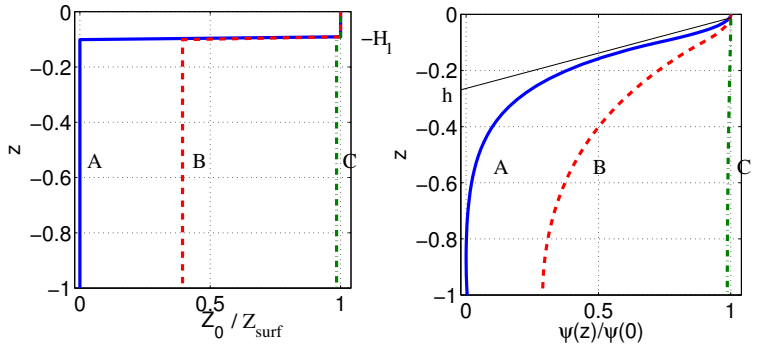


Figure 15. Left panel: three different vertical profiles of the microscopic enstrophy. Right panel: corresponding vertical structure of statistical equilibrium states ($\psi(z)/\psi(0)$ on the left panel), in the case of constant stratification ( $f_0^2/N^2 = 0.1$). The $e$-folding depth in case A is $h = f_0/NK$ (with here $K = 1$ for the statistical equilibrium state).

computed numerically in the case of arbitrary profiles $Z_0(z)$. Let us consider the example shown in figure 15, for a two-step microscopic enstrophy profile

$$Z_0 = Z_{\rm surf}\Theta\left(z + H_1\right) + Z_{\rm int}\Theta\left(-z - H_1\right), \quad H_1 \ll H, \tag{27}$$

where $\Theta$ is the Heaviside function, and for $Z_{\rm int}/Z_{\rm surf}$ varying between 0 and 1. We find that the minimum macroscopic enstrophy states are always characterized by the gravest horizontal mode on the horizontal ($K = 1$). As for the vertical structure, we observe figure 15 a tendency toward more barotropic flows when the ratio $Z_{\rm int}/Z_{\rm surf}$ tends to one. One can actually show that the equilibrium state is barotropic when $Z_{\rm int}/Z_{\rm surf} = 1$, and that the equilibrium state is surface intensified with $e$-folding depth $h = f_0/N(0)K$ when $Z_{\rm int}/Z_{\rm surf} = 0$ and $H_1 \ll H$, see Venaille *et al.* (2012).

These examples show the importance of the conservation of microscopic enstrophy $Z_0(z)$ to the vertical structure of the equilibrium state. The main result is that statistical mechanics predicts a tendency for the flow to reach the gravest Laplacian mode on the horizontal ($K = 1$). The vertical structure associated with this state is fully prescribed by solving (26) with $K = 1$. Because the barotropic component of such flows are larger than solutions of (26) with $K > 1$, we can say that the inverse cascade on the horizontal is associated with a tendency to reach the gravest vertical mode compatible with the vertical microscopic enstrophy profile $Z_0$. This means a tendency toward barotropization, although in general, the fact that the profile $Z_0$ is non constant prevents complete barotropization.

5.2.2. *Including the $\beta$-effect .*

For a given initial condition $\psi_0(x, y, z)$, increasing $\beta$ increases the contribution of the (depth independent) available potential enstrophy defined as

$$Z_p = \beta^2 \int_{\mathcal{D}} \mathrm{d}x\mathrm{d}y \; y^2, \tag{28}$$

to the total microscopic enstrophy profile $Z_0(z) = \int_{\mathcal{D}} \mathrm{d}x\mathrm{d}y \; q_0^2$, where $q_0$ is the initial potential vorticity field that can be computed by injecting $\psi_0$ in (20). For sufficiently large values of $\beta$, the potential vorticity field is dominated by the beta effect ($q_0 \approx \beta y$), $Z_0$ therefore tends to $Z_p$ and becomes depth independent. Because statistical equilibria computed in the previous subsection were fully barotropic when the microscopic enstrophy $Z_0$ was depth-independent, we expect a tendency toward barotropization by increasing $\beta$.

5.2.3. *Numerical experiments*

We consider in this section the final state organization of an initial surface intensified flow, varying the values of $\beta$. The initial potential vorticity field is $q_0 = q_{\mathrm{surf}}(x, y)\Theta\left(z + H_1\right) + \beta y$, such that $q_0 = \beta y$ in the interior ($-H < z < -H_1$) and $q_0 \approx q_{\mathrm{surf}}$ in a surface layer $z > -H_1$. The surface potential vorticity $q_{\mathrm{surf}}(x, y)$ is a random field with random phases in spectral space, and a Gaussian power spectrum peaked at wavenumber $K_0 = 5$, with variance $\delta K_0 = 2$, and normalized such that the total energy is equal to one ($E_0 = 1$).

We perform simulations of the dynamics by considering a vertical discretization with 10 layers of equal depth, horizontal discretization of $512^2$, $H = 1$, and $F = (Lf_0/HN)^2 = 1$, using a pseudo-spectral quasi-geostrophic model (Smith and Vallis, 2001). We choose $H_1 = H/10$ for the initial condition, so that there is non zero enstrophy only in the upper layer in the absence of a beta effect.

The case with $\beta = 0$ is presented in the left panel of figure 16. An inverse cascade in the horizontal leads to flow structures with an horizontal wavenumber $K$ decreasing with time, associated with a tendency toward barotropization: the $e$-folding depth of the surface-intensified flow increases as $f_0/2NK$. The concomitant horizontal inverse cascade (most of the kinetic energy is in the gravest horizontal mode $K = 1$ at the end of the simulation) and the increase of the $e$-folding depth are observed on figure 16, showing good qualitative agreement between statistical mechanics and

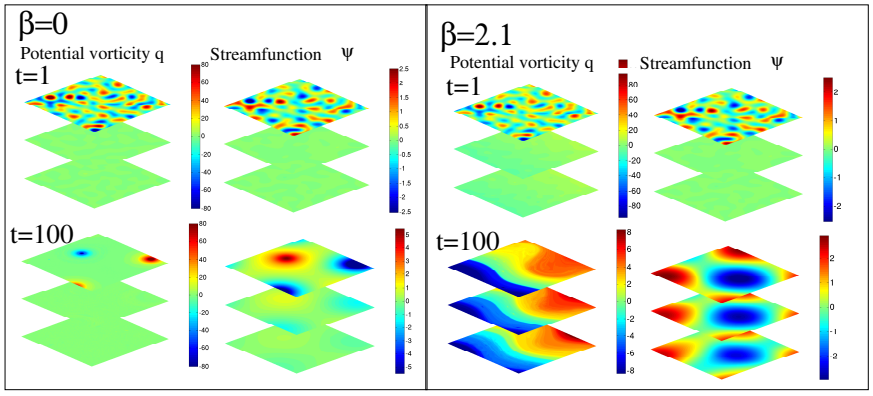


Figure 16. Left: case without beta plane. Only the fields in upper, middle and lower layer are shown. The end-state is surface-trapped. Right: case with a beta plane; the initial streamfunction is the same as on the left. The end-state is almost depth-independant. Note that the interior " beta plane" is not clearly visible in the upper panel of potential vorticity because the color scale is different than in the lower panel.

numerical simulations.

We now switch on the beta effect, with the same initial surface-intensified streamfunction $\psi_0(x, y, z)$. As a consequence, the contribution of the depth independent part of the microscopic enstrophy increases, which means a tendency toward a more barotropic equilibria, according to the previous subsection. This is what is actually observed in the final state organization of figure 16 in the presence of beta effect. This result reflects the fact that in physical space, the initial surface-intensified flow stirs the interior potential vorticity field (initially a beta plane), which in turn induces an interior flow, which stirs even more the interior potential vorticity field, and so on. We conclude that in this regime, the beta effect is a catalyst of barotropization, as predicted by statistical mechanics.

### 5.3. *The formation of bottom-trapped flows*

We saw in the previous section that the existence of planetary vorticity gradients (beta effect) provide a depth-independant source of microscopic enstrophy that favors barotropization. Another source of microscopic potential vorticity would be provided by the addition of bottom topography. This should in this case play against barotropization, since the topography induces potential microscopic enstrophy in the lower layer only. In fact, an initially surface intensified flow may evolve towards a bottom trapped

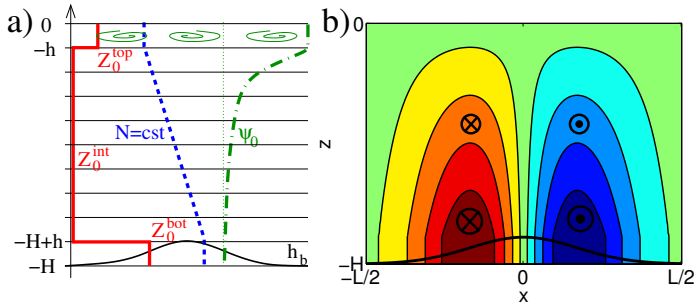


Figure 17. a) Sketch of the flow configuration. The continuous red line represents the initial microscopic enstrophy profile (here $Z_0^{int} = 0$). The dashed blue line represents the density profile, and the dashed-dotted green line represents the streamfunction amplitude shape, which is initially surface-intensified. The thick continuous black line represents bottom topography. b) Vertical slice of the meridional velocity field $v$ of the statistical equilibrium state in the low energy limit.

current above the topographic anomaly, which can be explained by the statistical mechanics arguments presented above.

Bottom-intensified flows are commonly observed along topographic anomalies in the ocean. A striking example is given by the Zapiola anticyclone, a strong recirculation about 500 km wide that takes place above a sedimentary bump in the Argentine Basin, where bottom-intensified velocities of order 0.1 m.s$^{-1}$ have been reported from *in situ* measurements (Saunders and King, 1995) and models (de Miranda *et al.*, 1999).

Phenomenological arguments for the formation of bottom-trapped flows were previously given by Dewar (1998) in a forced-dissipated case. A complementary point of view was given by Merryfield (1998), who computed critical states of equilibrium statistical mechanics for truncated dynamics. He observed that some of these states were bottom intensified in the presence of topography. Venaille (2012) showed how to find the equilibrium states among these critical states, how they depend on the initial microscopic enstrophy profile, and provided numerical evidence of the spontaneous self-organization into bottom-trapped flows. We summarize in the following the main results.

We consider the configuration of figure 17-a: the stratification is linear in the bulk ($N$ is constant for $-H+h < z < -h$), and homogeneous in two layers of thickness $h \ll H$ at the top and at the bottom, where $N = 0^+$. In these upper and lower layers, the streamfunction is depth independent, denoted by $\psi^{top}(x, y, t)$ and $\psi^{bot}(x, y, t)$, respectively. In these layers, the

dynamics is then fully described by the advection of the vertical average of the potential vorticity fields, denoted by $q^{top}(x,y,t)$ and $q^{bot}(x,y,t)$. The interior potential vorticity field is denoted by $q^{int}(x,y,z,t)$. For a given field $q^{top}, q^{int}, q^{bot}$, the streamfunction is obtained by inverting the following equations:

$$q^{top} - \beta y = \Delta \psi^{top} - \frac{f_0^2}{hN^2}\frac{\partial}{\partial z}\psi\Big|_{z=-h} , \tag{29}$$

$$q^{bot} - \beta y - f_0\frac{h_b}{h} = \Delta \psi^{bot} + \frac{f_0^2}{hN^2}\frac{\partial}{\partial z}\psi\Big|_{z=h-H} , \tag{30}$$

$$q^{int} - \beta y = \Delta \psi + \frac{f_0^2}{N^2}\frac{\partial^2}{\partial z^2}\psi \quad \text{for } -H+h<z<-h , \tag{31}$$

$$\psi^{top} = \psi(x,y,-h),\ \psi^{bot} = \psi(x,y,-H+h). \tag{32}$$

Equations (29-30) are obtained by averaging Eq. (20) in the vertical direction in the upper and the lower layers, respectively, and by using the boundary condition (21). In the following, the initial condition is a surface-intensified velocity field induced by a perturbation of the potential vorticity field confined in the upper layer:

$$q_0^{top} = \beta y + q_0^{pert} , \quad q_0^{int} = \beta y , \quad q_0^{bot} = \frac{f_0}{h}h_b + \beta y. \tag{33}$$

It is assumed in the following that $\beta y \ll q_0^{pert} \ll f_0 h_b/h$. The potential vorticity fields are therefore associated with microscopic enstrophies $Z_0^{int} \ll Z_0^{top} \ll Z_0^{bot}$. The macroscopic enstrophy minimizers of this configuration are computed in the Appendix of Venaille (2012) by solving the variational problem (24-25). The main result is that for a fixed topography, in the *low energy limit*, the equilibrium streamfunction is a bottom-intensified quasi-geostrophic flow such that bottom streamlines follow contours of topography with positive correlations, see figure 17-b.

The initial condition of figure 18-b is the the same surface-intensified velocity field as the one used in figure 16. After a few eddy turnover times, the enstrophy of the upper layer has cascaded towards small scales as shown by numerous filaments in figure 18-c, concomitantly with an increase of the horizontal energy length scale. As in the case without topography, this inverse energy cascade on the horizontal leads therefore to a deeper penetration of the velocity field, shown in figure 18-d. When this velocity field reaches the bottom layer, it starts to stir the bottom potential vorticity

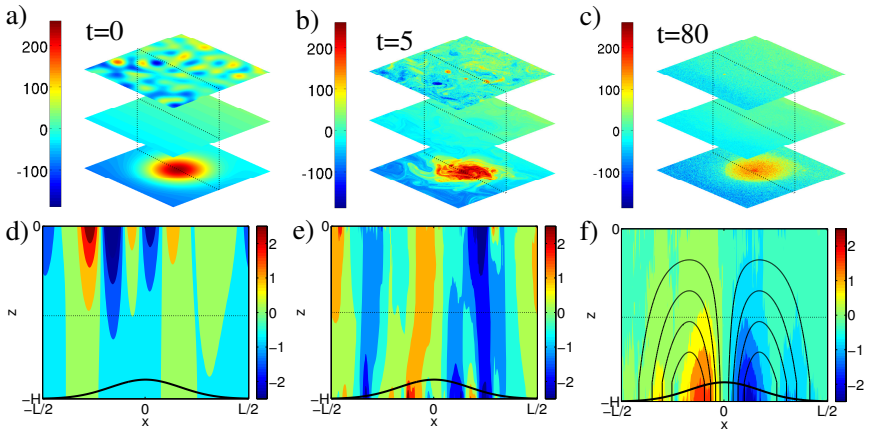


Figure 18. a),b),c) Potential vorticity field at three successive times. In each panel, only layers 1 (top), 5 (middle) and 10 (bottom) are represented. b),d),f) Vertical slices of the meridional velocity fields $v$ taken at the center of the domain ($y = 0$), and associated with the potential vorticity fields given in panels d),e),f), respectively. The bold continuous dark line represents bottom topography. The continuous black contours of panel f) give the structure of the statistical equilibrium state in the low energy (or large topography) limit, corresponding to figure 17-b. Contour intervals are the same as those between the different shades.

field. This induces a bottom-intensified flow, which then stirs the surface potential vorticity field, and so on. The corresponding flow is shown in figure 18-e, which clearly represents a bottom-intensified anticyclonic flow above the topographic anomaly, qualitatively similar to the one predicted by statistical mechanics in the low energy limit.

These results have important consequences for ocean energetics: topographic anomalies allow transferring surface-intensified eddy kinetic energy into bottom-trapped mean kinetic energy, which would eventually be dissipated in the presence of bottom friction, as for instance in the case of the Zapiola anticyclone (Dewar, 1998; Venaille *et al.*, 2011). In the case of the Zapiola anticyclone, the dissipation time scale is of the order of a few eddy turnover-time. It is therefore not *a priori* obvious that the results obtained in a freely evolving configuration may apply to this case. However, one can now build upon these results to address the role of forcing and dissipation in vertical energy transfers above topographic anomalies.

## 6. Conclusion

On these lectures, we have discussed applications of equilibrium statistical mechanics of the quasi-geostrophic model to the Great Red Spot and other vortices of Jupiter, to Jupiter's jets, to ocean mesoscale eddies, ocean mid-basin jets analogous to the Gulf-Stream or the Kuroshio, and to the vertical structure of geostrophic ocean turbulence.

All these applications illustrate the power of equilibrium statistical mechanics. The theory predicts the detailed shape, relation with both external and deep shear, and the jet profile for the Great Red Spot of Jupiter, depending on only a few key control parameters,. It also predicts the structure and the westward velocity of mesoscale vortices, much of the qualitative properties of mid-basin jets, and the vertical structure of quasi-geostrophic turbulence. Still more applications to ocean and atmosphere dynamics are currently under investigations.

However, the range of validity of the approach is limited. Equilibrium statistical mechanics can be valid only if the effects of forcing and dissipation can be neglected. This corresponds to two different kinds of situation. The first one, as discussed in the original papers (Robert, 1990; Miller, 1990; Robert, 1991; Robert and Sommeria, 1991), is when the flow is produced by an instability, or from a prepared initial condition, and then evolves to a self-organized state during a time scale which is much smaller than the typical time scales associated to the non-inertial processes (forcing and dissipation). This framework is probably the correct one, for instance for the formation of ocean mesoscale eddies from the instability either of the Gulf Stream (Gulf Stream rings) or of the Agulhas current downstream of Cape Agulhas.

Most of geophysical and other natural flows are however in another regime. Very often they have settled down from a very long time to a statistically stationary solution, for which forces balance dissipation on average. In this case, one can still compare the typical time scale for inertial organization on one hand (usually turnover times, or typical times for wave propagation) to the forcing and dissipation time scale on the other hand (spin up or spin down time scale). If these two time scales are well separated, then we still expect equilibrium statistical mechanics to describe at leading order the flow structure, and its qualitative properties. Usefulness of equilibrium statistical mechanics in this second framework, for instance close to a phase transition, is illustrated in (Bouchet and Simonnet, 2009). We nevertheless note a limitation of equilibrium statistical mechanics in

this second framework. It does not predict which of the set of possible statistical equilibria (parameterized by the inertial invariants) is actually selected by the long term effect of forces and dissipation. This should be determined at next order by computing the vanishingly small fluxes of conserved quantities.

Still most of ocean and atmosphere flows, for instance large scale organization of the atmosphere or the ocean, fulfill these separation of time scale hypothesis only marginally. Then a truly non-equilibrium statistical mechanics approach has to be considered. This is the subject of a number of current approaches, using kinetic theory (Nardini *et al.*, 2012; Bouchet and Morita, 2010), related approaches such as stochastic structural stability theory (see (Farrell and Ioannou, 2003, 2009; Srinivasan and Young, 2011) and references therein), or cumulant expansions (see (Marston, 2010; Marston *et al.*, 2008)and references therein), or instanton theory. Section 6 of the review (Bouchet and Venaille, 2012) contains a more complete discussion of such non-equilibrium approaches; whereas the review by (Marston, 2011) stresses the interest of statistical mechanics for climate applications.

## Acknowledgments

This work was supported through the ANR program STATFLOW (ANR-06-JCJC-0037-01) and through the ANR program STATOCEAN (ANR-09-SYSC-014), and partly by DoE grant DE-SC0005189 and NOAA grant NA08OAR4320752.

## References

Berloff, P., Hogg, A. M. and Dewar, W. (2007). The Turbulent Oscillator: A Mechanism of Low-Frequency Variability of the Wind-Driven Ocean Gyres, *Journal of Physical Oceanography* **37**, p. 2363.

Bouchet, F. (2001). *Mécanique statistique des écoulements géophysiques* (PHD, Université Joseph Fourier-Grenoble).

Bouchet, F. (2008). Simpler variational problems for statistical equilibria of the 2d euler equation and other systems with long range interactions, *Physica D Nonlinear Phenomena* **237**, pp. 1976–1981.

Bouchet, F., Chavanis, P. H. and Sommeria, J. (2012). Statistical mechanics of Jupiter's Great Red Spot in the shallow water model, *Preprint, to be submitted* .

Bouchet, F. and Dumont, T. (2003). Emergence of the great red spot of jupiter from random initial conditions, *cond-mat/0305206* .

Bouchet, F. and Morita, H. (2010). Large time behavior and asymptotic stability of the 2D Euler and linearized Euler equations, *Physica D Nonlinear Phenomena* **239**, pp. 948–966.

Bouchet, F. and Simonnet, E. (2009). Random Changes of Flow Topology in Two-Dimensional and Geophysical Turbulence, *Physical Review Letters* **102**, 9, p. 094504.

Bouchet, F. and Sommeria, J. (2002). Emergence of intense jets and Jupiter's Great Red Spot as maximum-entropy structures, *Journal of Fluid Mechanics* **464**, pp. 165–207.

Bouchet, F. and Venaille, A. (2012). Statistical mechanics of two-dimensional and geophysical flows, *Physics Reports* **515**, pp. 227–295.

Bretherton, F. (1966). Critical layer instability in baroclinic flows, *Quart. J. Roy. Meteor. Soc.* **92**, pp. 325–334.

Bretherton, F. P. and Haidvogel, D. B. (1976). Two-dimensional turbulence above topography, *Journal of Fluid Mechanics* **78**, pp. 129–154.

Callen, H. B. (1985). *Thermodynamics and an Introduction to Thermostatistics, 2nd Edition.*

Charney, J. G. (1971). Geostrophic Turbulence. *Journal of Atmospheric Sciences* **28**, pp. 1087–1094.

Chavanis, P. H. (2002). Statistical mechanis of two-dimensional vortices and stellar systems, in T. Dauxois, S. Ruffo, E. Arimondo and M. Wilkens (eds.), *Dynamics and Thermodynamics of Systems With Long Range Interactions*, *Lecture Notes in Physics*, Vol. 602 (Springer-Verlag), pp. 208–289.

Chavanis, P. H. and Sommeria, J. (1996). Classification of self-organized vortices in two-dimensional turbulence: the case of a bounded domain, *J. Fluid Mech.* **314**, pp. 267–297.

de Miranda, A. P., Barnier, B. and Dewar, W. K. (1999). On the dynamics of the Zapiola Anticyclone, *J. Geophys. Res.* **104**, pp. 21137 – 21150.

Dewar, W. (1998). Topography and barotropic transport control by bottom friction, *J. Mar. Res.* **56**, pp. 295–328.

Dibattista, M. T. and Majda, A. J. (2000). An Equilibrium Statistical Theory for Large-Scale Features of Open-Ocean Convection, *Journal of Physical Oceanography* **30**, pp. 1325–1353.

Dibattista, M. T., Majda, A. J. and Marshall, J. (2002). A Statistical Theory for the "Patchiness" of Open-Ocean Deep Convection: The Effect of Preconditioning, *Journal of Physical Oceanography* **32**, pp. 599–626.

Dowling, T. E. (1995). Dynamics of jovian atmospheres, *Annual Review of Fluid Mechanics* **27**, pp. 293–334.

Eyink, G. L. and Sreenivasan, K. R. (2006). Onsager and the theory of hydrodynamic turbulence, *Rev. Mod. Phys.* **78**, pp. 87–135.

Farrell, B. and Ioannou, P. J. (2009). A Theory of Baroclinic Turbulence, *Journal of the atmospheric sciences* **66**, 8, pp. 2444–2454.

Farrell, B. F. and Ioannou, P. J. (2003). Structural Stability of Turbulent Jets. *Journal of Atmospheric Sciences* **60**, pp. 2101–2118.

Ferrari, R. and Wunsch, C. (2009). Ocean Circulation Kinetic Energy: Reservoirs, Sources, and Sinks, *Annual Review of Fluid Mechanics* **41**, pp. 253–282.

Fofonoff, N. P. (1954). Steady flow in a frictionless homogeneous ocean. *J. Mar. Res.* **13**, pp. 254–262.

Gill, A. E. (1982). *Atmosphere-Ocean Dynamics.*

Gill, A. E., Green, J. S. A. and Simmons, A. (1974). Energy partition in the large-scale ocean circulation and the production of mid-ocean eddies, *Deep-Sea Research* **21**, pp. 499–528.

Hogg, N. G. and Stommel, H. M. (1985). The Heton, an Elementary Interaction Between Discrete Baroclinic Geostrophic Vortices, and Its Implications Concerning Eddy Heat-Flow, *Royal Society of London Proceedings Series A* **397**.

Ingersoll, A. P. and Vasavada, A. R. (1998). Dynamics of Jupiter's atmosphere. *IAU Special Session* **1**, pp. 1042–1049.

Kraichnan, R. H. and Montgomery, D. (1980). Two-dimensional turbulence, *Reports on Progress in Physics* **43**, pp. 547–619.

Landau, L. D. and Lifshitz, E. M. (1980). *Statistical Physics. Vol. 5 of the Course of Theoretical Physics* (Pergamon Press).

Lapeyre, G. (2009). What Vertical Mode Does the Altimeter Reflect? On the Decomposition in Baroclinic Modes and on a Surface-Trapped Mode, *Journal of Physical Oceanography* **39**, p. 2857.

Lim, C. and Nebus, J. (2007). *Vorticity, Statistical Mechanics, and Monte Carlo Simulation*, Springer Monographs in Mathematics (ISSN 1439-7382) (New York, NY : Springer Science+Business Media).

Majda, A. J. and Wang, X. (2006). *Nonlinear Dynamics and Statistical Theories for Basic Geophysical Flows* (Cambridge University Press).

Marcus, P. S. (1993). Jupiter's Great Red Spot and other vortices, *Ann. Rev. Astron. Astrophys.* **31**, pp. 523–573.

Marston, B. (2011). Looking for new problems to solve? Consider the climate, *Physcs Online Journal* **4**, 20.

Marston, J. B. (2010). Statistics of the general circulation from cumulant expansions, *Chaos* **20**, 4, p. 041107.

Marston, J. B., Conover, E. and Schneider, T. (2008). Statistics of an Unstable Barotropic Jet from a Cumulant Expansion, *Journal of Atmospheric Sciences* **65**, p. 1955.

Merryfield, W. J. (1998). Effects of stratification on quasi-geostrophic inviscid equilibria, *Journal of Fluid Mechanics* **354**, pp. 345–356.

Michel, J. and Robert, R. (1994). Large deviations for young measures and statistical mechanics of infinite dimensional dynamical systems with conservation law, *Communications in Mathematical Physics* **159**, pp. 195–215.

Miller, J. (1990). Statistical mechanics of euler equations in two dimensions, *Phys. Rev. Lett.* **65**, 17, pp. 2137–2140, doi:10.1103/PhysRevLett.65.2137.

Modica, L. (1987). The gradient theory of phase transitions and the minimal interface criterion, *Archive for Rational Mechanics and Analysis* **98**, pp. 123–142, doi:10.1007/BF00251230.

Nardini, C., Gupta, S., Ruffo, S., Dauxois, T. and Bouchet, F. (2012). Kinetic theory for non-equilibrium stationary states in long-range interacting systems, *Journal of Statistical Mechanics: Theory and Experiment* **1**, p. 0.

Onsager, L. (1949). Statistical hydrodynamics, *Nuovo Cimento* **6 (No. 2 (Suppl.))**, pp. 249–286.

Pedlosky, J. (1982). *Geophysical fluid dynamics.*

Pedlosky, J. (1998). *Ocean Circulation Theory* (New York and Berlin, Springer-Verlag).

Rhines, P. (ed.) (1977). *The dynamics of unsteady currents*, Vol. 6 (Wiley and Sons).

Robert, R. (1990). Etats d'équilibre statistique pour l'écoulement bidimensionnel d'un fluide parfait, *C. R. Acad. Sci.* **1**, pp. 311:575–578.

Robert, R. (1991). A maximum-entropy principle for two-dimensional perfect fluid dynamics, *J. Stat. Phys.* **65**, pp. 531–553.

Robert, R. and Sommeria, J. (1991). Statistical equilibrium states for two-dimensional flows, *J. Fluid Mech.* **229**, pp. 291–310.

Salmon, R. (1998). *Lectures on Geophysical Fluid Dynamics* (Oxford University Press).

Salmon, R., Holloway, G. and Hendershott, M. C. (1976). The equilibrium statistical mechanics of simple quasi-geostrophic models, *Journal of Fluid Mechanics* **75**, pp. 691–703.

Saunders, P. M. and King, B. A. (1995). Bottom Currents Derived from a Shipborne ADCP on WOCE Cruise A11 in the South Atlantic, *Journal*

*of Physical Oceanography* **25**, pp. 329–347.

Scott, R. B. and Wang, F. (2005). Direct Evidence of an Oceanic Inverse Kinetic Energy Cascade from Satellite Altimetry, *Journal of Physical Oceanography* **35**, p. 1650, doi:10.1175/JPO2771.1.

Smith, K. S. (2007). The geography of linear baroclinic instability in Earth's oceans, *Journal of Marine Research* **65**, pp. 655–683.

Smith, K. S. and Vallis, G. K. (2001). The Scales and Equilibration of Midocean Eddies: Freely Evolving Flow, *Journal of Physical Oceanography* **31**, pp. 554–571, doi:10.1175/1520-0485(2001)031.

Sommeria, J. (2001). Two-Dimensional Turbulence, in S. Berlin (ed.), *New trends in turbulence*, *Les Houches*, Vol. 74, pp. 385–447.

Sommeria, J., Nore, C., Dumont, T. and Robert, R. (1991). Statistical theory of the Great Red SPOT of Jupiter, *Academie des Science Paris Comptes Rendus Serie B Sciences Physiques* **312**, pp. 999–1005.

Srinivasan, K. and Young, W. R. (2011). Zonostrophic Instability, *Journal of the atmospheric sciences* **69**, 5, pp. 1633–1656.

Tabeling, P. (2002). Two-dimensional turbulence: a physicist approach, *Physics Reports* **362**, pp. 1–62.

Turkington, B. (1983). On steady vortex flow in two dimensions, I, *Communications in Partial Differential Equations* **8 (9)**, pp. 999–1030.

Turkington, B., Majda, A., Haven, K. and Dibattista, M. (2001). Statistical equilibrium predictions of jets and spots on Jupiter, *PNAS* **98**, pp. 12346–12350.

Vallis, G. K. (2006). *Atmospheric and Oceanic Fluid Dynamics*, doi: 10.2277/0521849691.

Venaille, A. (2012). Bottom-trapped currents as statistical equilibrium states above topographic anomalies, *Journal of Fluid Mechanics* **699**, pp. 500–510.

Venaille, A. and Bouchet, F. (2009). Statistical Ensemble Inequivalence and Bicritical Points for Two-Dimensional Flows and Geophysical Flows, *Physical Review Letters* **102**, 10, p. 104501.

Venaille, A. and Bouchet, F. (2011a). Ocean rings and jets as statistical equilibrium states, *Journal of Physical Oceanography* **10**, pp. 1860–1873.

Venaille, A. and Bouchet, F. (2011b). Solvable Phase Diagrams and Ensemble Inequivalence for Two-Dimensional and Geophysical Turbulent Flows, *Journal of Statistical Physics* **143**, pp. 346–380.

Venaille, A., Le Sommer, J., Molines, J. and Barnier, B. (2011). Stochastic variability of oceanic flows above topography anomalies. *Geophysical Research Letters* **38**, 16611.

Venaille, A., Vallis, G. and Griffies, S. (2012). The catalytic role of the beta effect in barotropization processes, *Journal of Fluid Mechanics* .

Wang, J. and Vallis, G. K. (1994). Emergence of Fofonoff states in inviscid and viscous ocean circulation models, *Journal of Marine Research* **52**, pp. 83–127.